JBC RESEARCH ARTICLE

Acetylation of calmodulin regulates synaptic plasticity and fear learning

Received for publication, March 2, 2021, and in revised form, July 20, 2021 Published, Papers in Press, July 31, 2021,
https://doi.org/10.1016/j.jbc.2021.101034

Hai-Long Zhang[1,2,‡], **Bing Zhao**[1,‡], **Wei Han**[1,‡], **Yi-Bei Sun**[1], **Pin Yang**[1], **Yongjun Chen**[3], **Duan Ni**[4], **Jian Zhang**[4], and **Dong-Min Yin**[1,*]

From the [1]Key Laboratory of Brain Functional Genomics, Ministry of Education and Shanghai, School of Life Science, East China Normal University, Shanghai, China; [2]Jiangsu Key Laboratory of Neuropsychiatric Diseases and Institute of Neuroscience, Soochow University, Suzhou, China; [3]Medical College of Acu-Moxi and Rehabilitation, Guangzhou University of Chinese Medicine, Guangzhou, China; [4]Key Laboratory of Cell Differentiation and Apoptosis of Chinese Ministry of Education, Department of Pharmacy, Clinical and Fundamental Research Center, Renji Hospital, Shanghai Jiao-Tong University School of Medicine (SJTU-SM), Shanghai, China

Edited by Roger Colbran

Synaptic plasticity is critical for brain function, including learning and memory. It is regulated by gene transcription and protein synthesis as well as posttranslational modifications at synapses. Although protein acetylation has been shown to be involved in the regulation of synaptic plasticity, this was mainly for histone protein acetylation. To investigate whether acetylation of nonhistone proteins is important for synaptic plasticity, we analyzed mouse brain acetylome and found that calmodulin (CaM), a ubiquitous Ca^{2+} sensor, was acetylated on three lysine residues, which were conserved across species. NMDA receptor-dependent long-term potentiation (LTP) is considered the most compelling form of synaptic plasticity. During LTP induction, activation of NMDA receptor triggers Ca^{2+} influx, and the Ca^{2+} binds with CaM and activates calcium/calmodulin-dependent protein kinase IIα (CaMKIIα), which is essential for LTP induction. By using home-generated and site-specific antibodies against acetylated CaM, we show that CaM acetylation is upregulated by neural activities in an NMDA receptor-dependent manner. Moreover, mutation of acetyllysines in CaM1 proteins disrupts synaptic plasticity and fear learning in a mouse model. We further demonstrate that acetylation of CaM reduces the binding free energy and increases the binding affinity toward CaMKIIα, a protein kinase pivotal to synaptic plasticity and learning. Taken together, our results demonstrate importance of CaM acetylation in regulating synaptic plasticity and learning.

Synaptic plasticity is critical for several brain functions including learning and memory. It is regulated by long-term mechanisms such as gene transcription (1, 2), as well as acute mechanisms at synapses including local protein synthesis (3), neurotransmitter receptor trafficking (4–6), and protein phosphorylation (7, 8). Calcium signaling is essential for synaptic plasticity and is initiated by activation of ion channels such as NMDA receptor and voltage-dependent Ca^{2+} channels (VDCC) and is mediated through several Ca^{2+}-binding proteins such as calmodulin (CaM), S100 family proteins, synaptotagmin (SYT), and protein kinase C (PKC) (9–13).

CaM is a ubiquitous Ca^{2+} sensor and has more than 300 target proteins including protein kinases, enzymes, cytoskeleton proteins, ion and water channels (14–19). For instance, CaM interacts with and activates Ca^{2+}/calmodulin-dependent protein kinase IIα (CaMKIIα) and protein phosphatase calcineurin (CaN), which are important for several cellular functions including plasticity and learning in the brain (14, 20–23). In addition, the conformational change of CaM upon binding with Ca^{2+} has been utilized to generate fluorescence proteins to monitor the activity of excitable cells (24).

Protein acetylation is regulated by lysine acetyltransferase (KAT) and lysine deacetylase (KDAC) and was discovered initially as a posttranslational modification of histone proteins to activate gene transcription (25). In accord, histone protein acetylation has been implicated in diverse physiological conditions including synaptic plasticity and learning (26–30). On the other hand, acetylation of nonhistone proteins has been shown to regulate a plethora of biological processes such as DNA repair, cytoskeleton dynamics, cell metabolism, and autophagy (31–36). However, the roles of nonhistone protein acetylation in synaptic plasticity and learning are less well understood (37).

In analyzing the mouse brain acetylome, we found that CaM was heavily acetylated. By using home-generated and site-specific antibodies against acetylated CaM, we show that CaM acetylation is increased within minutes of LTP (long-term potentiation) induction, but not LTD (long-term depotentiation), in a manner dependent on NMDA receptor activation. Mutation of acetyllysines in CaM1 proteins impairs hippocampal LTP and contextual fear learning. The mechanistic study indicates that acetylation of CaM reduces the binding free energy and increases the binding affinity toward CaMKIIα, a protein kinase pivotal to synaptic plasticity and learning. Together, our results reveal important roles of CaM acetylation in synaptic plasticity and learning.

‡ These authors contributed equally to this work.
* For correspondence: Dong-Min Yin, dmyin@brain.ecnu.edu.cn.

Results

Increase of CaM acetylation by neural activities

CaM is a ubiquitous calcium sensor and plays important roles in calcium signaling and synaptic plasticity (38–40). Previous proteomic studies have identified CaM acetylation in several tissues including the blood, liver, heart, lung, and brain (33, 36, 41, 42). However, the function and regulation of CaM acetylation remain largely unknown. To investigate whether CaM acetylation is regulated by neural activities, we analyzed two paradigms—chemical LTP (cLTP) stimulation *in vitro* and contextual fear learning *in vivo*, both of which can activate calcium signaling through NMDA receptor (43, 44). When hippocampal slices were stimulated with 50 μM forskolin and 100 nM rolipram for 15 min, LTP can be induced at Schaffer collateral (SC)-CA1 synapses (Fig. 1*A*) (43). Acetylated proteins were precipitated with anti-Ac-K antibody and probed by anti-CaM antibody. cLTP-induced CaM acetylation (Ac-CaM) occurred within minutes of the stimulation, but returned to basal levels by 30 min after washout of cLTP stimulation (Fig. 1, *B* and *C*). The potentiation effect of cLTP on CaM acetylation was specific because it was not observed in hippocampal slices

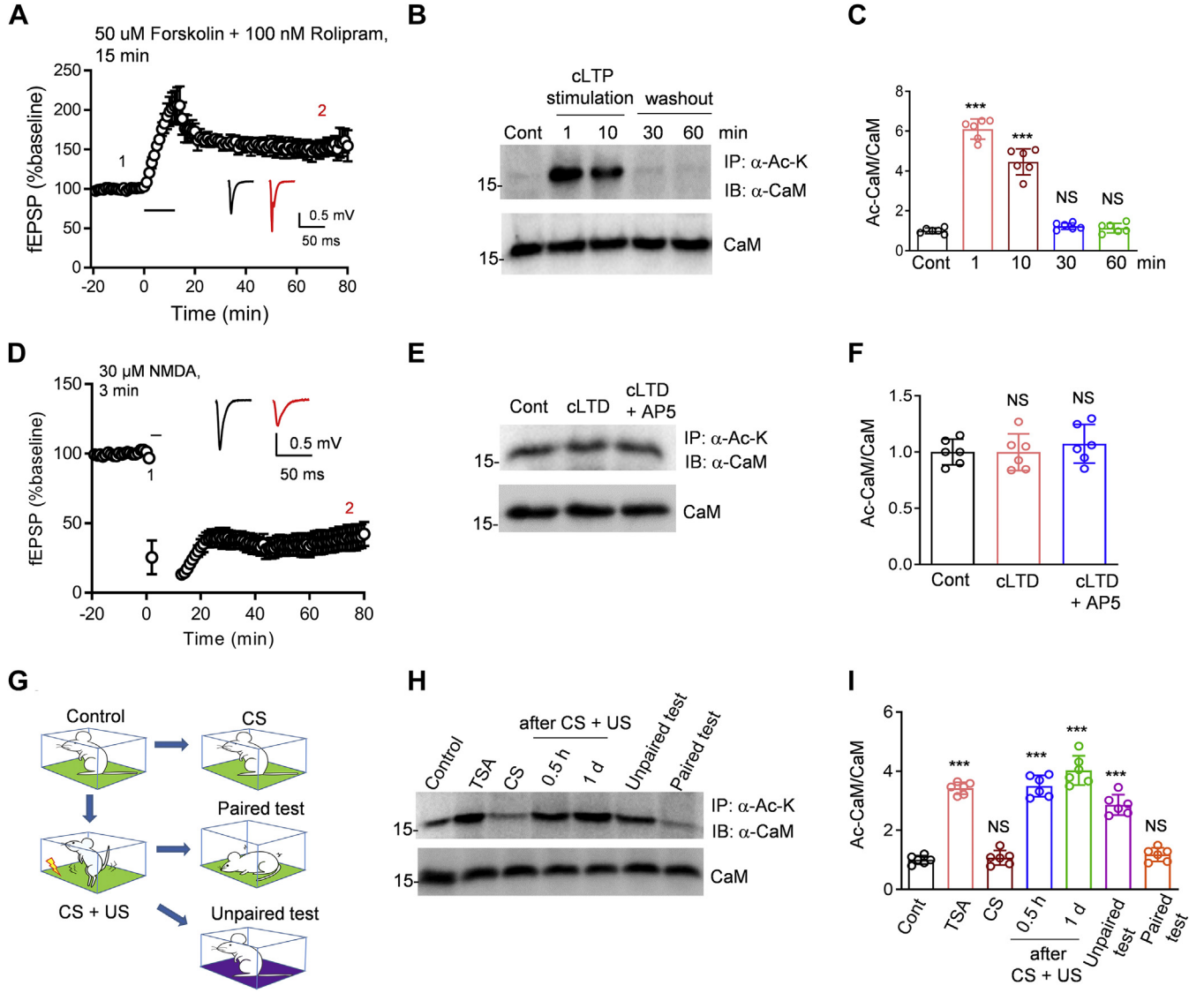

Figure 1. Upregulation of CaM acetylation by neural activities. *A*, increased fEPSP amplitudes at SC-CA1 synapses by forskolin and rolipram treatment (indicated by the bar), n = 3. *B*, time-dependent CaM acetylation in hippocampal slices in response to cLTP stimulation. The total lysates from hippocampal slices were immunoprecipitated by anti-acetyllysine antibodies and then were immunoblotted with anti-CaM antibodies. The lower CaM blots were of input samples. *C*, quantification of Ac-CaM/CaM in panel *B*. Data were represented as mean ± SD. ***$p < 0.0001$, compared with control, one-way ANOVA, n = 6, data were normalized to control. *D*, decreased fEPSP amplitudes at SC-CA1 synapses by 30 μM NMDA treatment for 3 min (indicated by the bar), n = 4. *E*, no effects of cLTD stimulation on Ac-CaM. The total lysates of hippocampal slices were immunoprecipitated by anti-acetyllysine antibodies and then were immunoblotted with anti-CaM antibodies. The lower CaM blots were of input samples. *F*, quantification of Ac-CaM/CaM in panel *E*. Data were represented as mean ± SD. NS, not significant, compared with controls, one-way ANOVA, n = 6. *G*, schematic diagrams of contextual fear conditioning tests. *H*, increased CaM acetylation during fear learning. The total lysates of hippocampus were immunoprecipitated by anti-acetyllysine antibodies and then were immunoblotted with anti-CaM antibodies. The lower CaM blots were of input samples. *I*, quantification of Ac-CaM/CaM in panel *H*. Data were represented as mean ± SD. ***$p < 0.0001$, compared with control, one-way ANOVA, n = 6, data were normalized to control. CS, conditioned stimulus (contextual box); US, unconditioned stimulus (foot shock).

stimulated by a paradigm that elicited chemical LTD (Fig. 1, *D–F*).

To study whether CaM acetylation is regulated by hippocampus-dependent contextual fear learning, mice were subjected to training (*i.e.*, pairing with the US—electric shock and CS—contextual box) and 1 day later, freezing or fear memory was tested when mice were returned to the contextual box (Fig. 1*G*). Of mice in the test box without electric shock (CS, contextual box), hippocampal Ac-CaM was similar to control (Fig. 1, *H* and *I*). However, their levels in the hippocampus were upregulated after pairing CS with US, almost as high as in mice injected with TSA, a KDAC inhibitor (Fig. 1, *H* and *I*). Ac-CaM remained high when mice were exposed to a new environment (*i.e.*, unpaired tests) (Fig. 1, *H* and *I*). By contrast, Ac-CaM returned to control levels after paired tests (*i.e.*, exposed to contextual box where they received electric shock) (Fig. 1, *H* and *I*). These results suggest that CaM acetylation is increased during contextual fear learning.

Increased CaM acetylation on K22, 95, and 116 by neural activities

By analyzing the previous proteomic studies (45, 46) and publicly available database (https://www.phosphosite.org/curatedInfoAction.action?record=9921012), we found that in mouse brain, CaM was acetylated on three lysine residues (K22, K95, and K116) that are conserved across species (Fig. 2*A*). To determine which of the three lysine residues in CaM could be acetylated, we generated site-specific antibodies against Ac-CaM at K22, K95, and K116. To demonstrate the specificity of the anti-Ac-CaM antibodies, we purified site-specifically acetylated recombinant CaM proteins using the strategy of genetic code expansion (Fig. 2*B*). This strategy uses an engineered pyrrolysyl-tRNA synthetase specific for Ac-K and its cognate $tRNA^{Pry}$ to incorporate Ac-K at an assigned codon to produce site-specifically acetylated proteins (47). As shown in Figure 2*C*, the pan-anti-Ac-K antibody can detect CaM acetylated at any of the three lysine residues. However, the anti-Ac-K22-CaM antibody only recognized CaM acetylated at K22, but not WT-CaM or CaM acetylated at K95 or K116, and vice versa (Fig. 2*C*). These results demonstrate the specificity of the anti-Ac-CaM antibodies.

We probed the total lysates of hippocampal slices with these antibodies. As shown in Figure 3, *A–D*, CaM acetylation at K22, K95, and K116 was increased by cLTP stimulation for 10 min. In addition, the induced acetylation was diminished by AP5, an antagonist of NMDA receptor, suggesting its dependence on NMDA receptor activation (Fig. 3, *A–D*). We used purified Ac-CaM proteins as standards to analyze the stoichiometry levels for each lysine residue under control and cLTP conditions. The stoichiometry levels of K22, K95, and K116 in the total lysates are 2.80%, 2.76%, 2.87% under basal conditions and are increased to 6.77%, 7.33%, 5.84% after cLTP stimulation (Fig. 3, *E–G*). The stoichiometry results showed that cLTP upregulated acetylation at individual lysine residue to 2- to 3-fold, which are consistent with the western blot results using the site-specific antibodies (Fig. 3, *A–D*). Taken together, these results demonstrate that CaM acetylation is upregulated by cLTP in a manner dependent on NMDA receptor activation.

To study whether the protein levels of Ac-CaM are increased in the synapse or nucleus after cLTP stimulation, we purified postsynaptic density (PSD) and nuclear fractions from hippocampal slices. Ac-CaM was upregulated in the PSD fraction of hippocampal slices after cLTP stimulation for 10 min, which was prevented by AP5 (Fig. 3, *H–K*). By contrast, acetylation of CaM was not elevated in the nucleus of hippocampal slices after cLTP stimulation for 10 min (Fig. S1). These results indicate that Ac-CaM was increased in the synapse after cLTP stimulation in an NMDAR-dependent way.

Next, we investigate whether CaM acetylation at the three lysine residues could be regulated by contextual fear learning. Mice were subjected to training (*i.e.*, pairing with the US—foot shocks and CS—contextual box) and 1 day later, freezing or fear memory was tested when mice were returned to the contextual box (Fig. 1*G*). Protein levels of Ac-CaM at K22, 95,

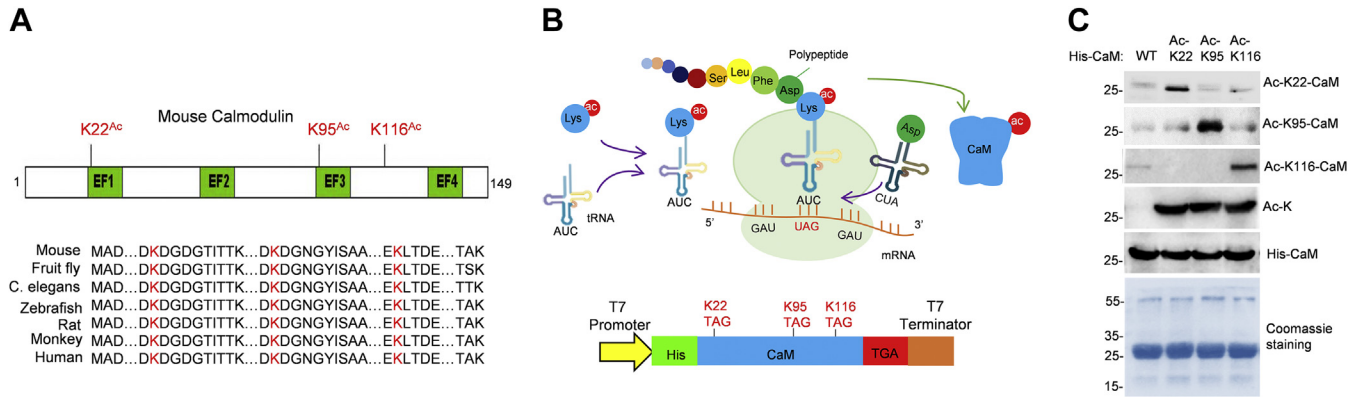

Figure 2. Generation and verification of site-specifically anti-Ac-CaM antibodies. *A*, *top*, diagram showing the position of acetyllysines in mouse CaM. *Numbers* represent amino acids. *Bottom*, alignment of the amino acid sequence of CaM from different species. K in *red color* indicates acetyllysines. *B*, *top*, diagram showing the strategy of genetic code expansion used to generate site-specifically acetylated recombinant CaM proteins. *Bottom*, schematic diagram of pCDF constructs expressing His-tagged acetylated CaM proteins in bacteria. *C*, western blot analysis to verify the specificity of anti-Ac-CaM antibodies. His-tagged WT-CaM and acetylated CaM proteins were probed with the indicated antibodies. EF, EF hands.

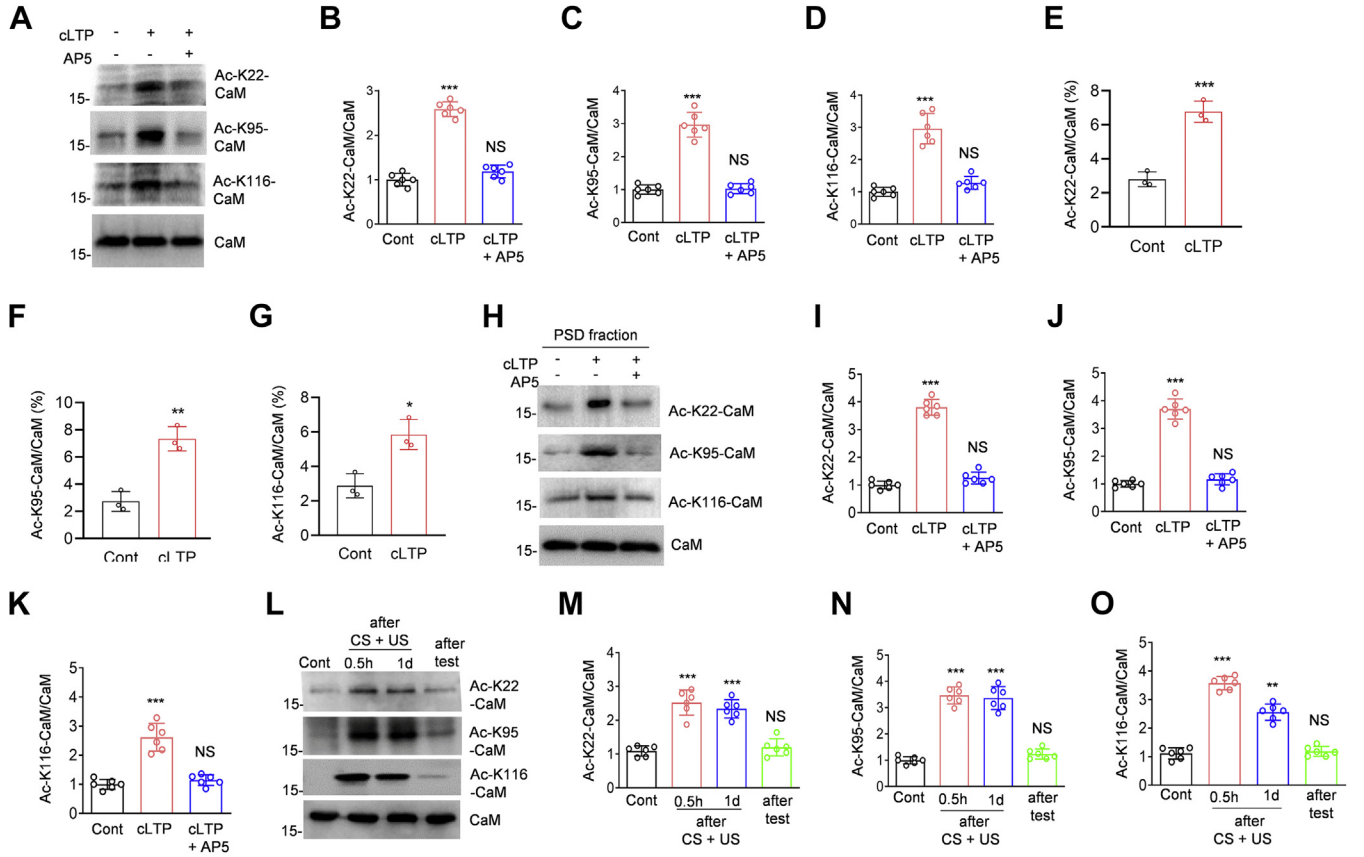

Figure 3. Increase of CaM acetylation on K22, 95, and 116 by neural activities. *A*, increased CaM acetylation at different lysine residues 10 min after cLTP stimulation in hippocampal slices without or with AP5. *B–D*, quantification of Ac-K22-CaM/CaM (*B*), Ac-K95-CaM/CaM (*C*), and Ac-K116-CaM/CaM (*D*) in panel *A*. Data were represented as mean ± SD. NS, not significant, ***$p < 0.0001$, compared with controls, one-way ANOVA, n = 6, data were normalized to control. *E–G*, stoichiometry levels of Ac-K22-CaM (*E*), Ac-K95-CaM (*F*), and Ac-K116-CaM (*G*) from control and cLTP-stimulated hippocampal slices. Data were represented as mean ± SD. ***$p = 0.0008$, **$p = 0.0023$, *$p = 0.01$, *t* test, n = 3. *H*, increased CaM acetylation at different lysine residues 10 min after cLTP stimulation in PSD fraction without or with AP5. The homogenates of hippocampal PSD fraction were probed with the indicated antibodies. *I–K*, quantification of Ac-K22-CaM/CaM (*I*), Ac-K95-CaM/CaM (*J*), and Ac-K116-CaM/CaM (*K*) in panel *H*. Data were represented as mean ± SD. NS, not significant, ***$p < 0.0001$, compared with controls, one-way ANOVA, n = 6, data were normalized to control. *L*, increased CaM acetylation at different lysine residues after pairing US and CS. The total lysates of hippocampus were probed with the indicated antibodies. *M–O*, quantification of Ac-K22-CaM/CaM (*M*), Ac-K95-CaM/CaM (*N*), and Ac-K116-CaM/CaM (*O*) in panel *L*. Data were represented as mean ± SD. NS, not significant, ***$p < 0.0001$, compared with controls, one-way ANOVA, n = 6, data were normalized to control.

and 116 in the hippocampus were upregulated after pairing CS with US, compared with control mice in the contextual box without foot shocks (Fig. 3, *L–O*). By contrast, protein levels of Ac-CaM at K22, 95, and 116 returned to control levels after paired tests (*i.e.*, exposed to contextual box where they received foot shocks) (Fig. 3, *L–O*). These results suggest that contextual fear learning increases the acetylation of CaM at the three lysine residues.

Increase of CaMKIIα activity by acetylation-mimicking CaM

To determine whether acetylation alters the interaction between CaM and CaMKIIα, we generated 3KR-CaM and 3KQ-CaM where the three lysine residues were mutated to arginine and glutamine, respectively to block and mimic acetylation (41, 48). K to Q mutation neutralizes the positive charge of K and is commonly used to be a mimic of acetyllysine (41, 48). We used 1 μM GST-CaM and His-CaMKIIα for the GST-pull-down assay in the presence of 0.1 mM Ca^{2+}. We finished the pull-down assay within 2 h but not overnight to avoid the saturation of CaMKIIα binding due to the long-time incubation. As shown in Figure 4*A*, GST-tagged WT-CaM was able to pull down His-CaMKIIα in a calcium-dependent manner. However, this interaction was inhibited by the KR mutation, but potentiated by the KQ mutation (Fig. 4, *A* and *B*). These results suggest that acetylation-resistant CaM reduces while acetylation-mimicking CaM enhances the interaction with CaMKIIα, compared with WT-CaM.

Next, we determine whether acetylation-mimicking CaM could enhance the kinase activity of CaMKIIα by an assay of *in vitro* CaMKIIα autophosphorylation—with purified His-CaMKIIα and GST-tagged WT or mutant CaM. We used 1 μM GST-CaM and His-CaMKIIα for the assay in the presence of 0, 0.004, or 0.1 mM Ca^{2+}. Autophosphorylated CaMKIIα was detected with phospho-specific antibody against Thr^{286}, whose phosphorylation is an indicator of CaMKIIα activation (49). CaMKIIα became activated by incubation with GST-CaM in a Ca^{2+}-dependent manner (Fig. 4*C*). Remarkably, p-CaMKIIα was reduced by 3KR-CaM, but increased by 3KQ-CaM (Fig. 4, *C–F*). Note that acetylation-mimicking CaM had no effects on the interaction with CaN or its phosphatase activity (Fig. S2), indicating the specificity of CaM acetylation to

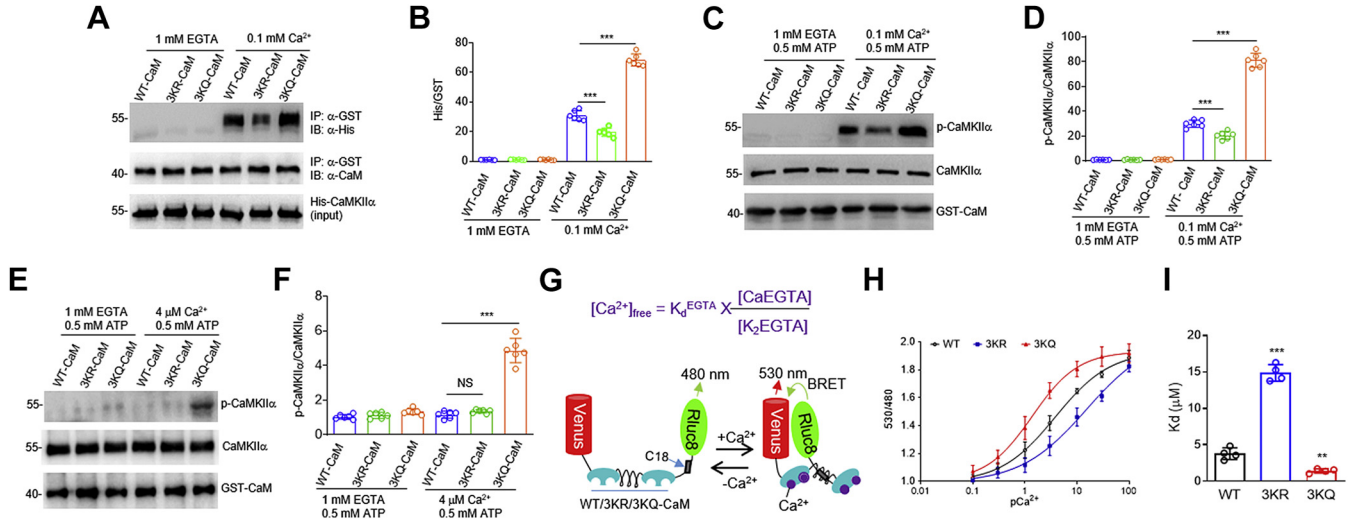

Figure 4. Increase of CaMKIIα activity by acetylation-mimicking CaM. *A*, CaMKIIα interaction was reduced by 3KR, but increased by 3KQ. His-CaMKIIα and GST-tagged WT and mutant CaM were purified from bacteria and tested for interaction in the presence of 1 mM EGTA or 0.1 mM Ca^{2+}. *B*, quantification of band intensities (His/GST) in panel *A*. Data were represented as mean ± SD. ***$p < 0.0001$, two-way ANOVA followed by Tukey's multiple comparisons test, n = 6, data were normalized to WT-CaM in the presence of 1 mM EGTA. *C*, CaMKIIα activity was reduced by 3KR, but increased by 3KQ. Flag-CaMKIIα and GST-tagged WT and mutant CaM were purified from bacteria and incubated in the presence of 1 mM EGTA or 0.1 mM Ca^{2+}. CaMKIIα activity was revealed by anti-p-CaMKIIα. *D*, quantification of p-CaMKIIα/CaMKIIα in panel *C*. Data were represented as mean ± SD. ***$p < 0.0001$, two-way ANOVA followed by Tukey's multiple comparisons test, n = 6, data were normalized to WT-CaM in the presence of 1 mM EGTA. *E*, Ca^{2+}-dependent CaMKIIα activation by 3KQ-CaM. Assay was done as in panel *C*, but in the presence of 1 mM EGTA or 4 μM Ca^{2+}. *F*, quantification of p-CaMKIIα/CaMKIIα in panel *E*. Data were represented as mean ± SD. NS, not significant, ***$p < 0.0001$, two-way ANOVA followed by Tukey's multiple comparisons test, n = 6, data were normalized to WT-CaM in the presence of 1 mM EGTA. *G*, diagram showing the principle of BRET assay to study the interaction between CaM and the target peptide from CaMKIIα (C18). *H*, 3KR decreased while 3KQ increased binding affinity between CaM and CaMKIIα. Shown is the binding curve between WT, 3KR, 3KQ-CaM, and C18 under different concentration of Ca^{2+}. The x-axis represents the Ca^{2+} concentration scaled by log_{10}, the y-axis indicates the value of 530/480. Data were represented as mean ± SD. $p = 0.0003$, F (2,9) = 22.13, two-way ANOVA, n = 4, data were normalized to 0 μM Ca^{2+}. *I*, quantification of Kd value of the interaction between WT, 3KR, 3KQ-CaM, and C18. Data were represented as mean ± SD. **$p = 0.0053$, ***$p < 0.0001$, compared with WT, one-way ANOVA, n = 4.

activate CaMKIIα. Taken together, these results demonstrate that acetylation-resistant CaM reduces while acetylation-mimicking CaM increases the kinase activity of CaMKIIα, compared with WT-CaM.

To explore how acetylation-mimicking CaM affects the interaction with CaMKIIα, we performed bioluminescence resonance energy transfer (BRET) analysis. HEK293 cells were transfected with a BRET construct encoding Venus (a yellow fluorescent protein), CaM, C18 (a CaM binding peptide from CaMKIIα), and RLuc8 (enhanced Renilla luciferase) (Fig. 4*G*) (modified from a previous report (50)). Compared with WT-CaM (K_d = 3.92 ± 0.08 μM), 3KR-CaM had a right-shifted binding curve and a higher K_d value (14.41 ± 0.98 μM) while 3KQ-CaM exhibited a left-shifted binding curve and a lower K_d value (1.39 ± 0.01 μM) (Fig. 4, *H* and *I*). These results indicate that 3KR-CaM decreases while 3KQ-CaM increases the binding affinity toward CaMKIIα, compared with WT-CaM. By contrast, 3KR and 3KQ-CaM show the similar binding affinity toward myosin light chain kinase (MLCK) in the BRET assay (Fig. S3), demonstrating the specificity on CaMKIIα interaction. Altogether, these data demonstrate that acetylation-mimicking CaM has a higher binding affinity with CaMKIIα, compared with WT-CaM.

Promotion of CaMKIIα activity by acetylated CaM

To further study whether CaM acetylation promotes the interaction with CaMKIIα, we generated site-specifically acetylated recombinant CaM proteins using the strategy of genetic code expansion (Fig. 2*B*). We purified His-tagged WT-CaM and acetylated CaM at the three lysine residues (Ac-3K-CaM) (Fig. 5*A*). Note that WT-CaM purified from bacteria could not be acetylated (Figs. 2*C* and 5*A*). His-tagged WT or Ac-3K-CaM was incubated with Flag-CaMKIIα purified from HEK293 cells for coimmunoprecipitation (Co-IP) experiments. Similar with the GST pull-down assay with 3KQ-CaM, we used 1 μM His-CaM and Flag-CaMKIIα for the Co-IP experiments in the presence of 0.1 mM Ca^{2+}. We finished the Co-IP experiments within 2 h but not overnight to avoid the saturation of CaMKIIα binding due to the long-time incubation. As shown in Figure 5*B*, WT-CaM was able to interact with Flag-CaMKIIα in the presence of 0.1 mM Ca^{2+}. However, this interaction was potentiated by Ac-3K-CaM (Fig. 5, *B* and *C*), suggesting that CaM acetylation promotes the CaM-CaMKIIα interaction.

We next determine whether acetylated CaM increases the kinase activity of CaMKIIα by an assay of *in vitro* CaMKIIα autophosphorylation—with purified Flag-CaMKIIα and different forms of His-CaM. Similar with the assay with 3KQ-CaM, we used 1 μM His-CaM and Flag-CaMKIIα for the assay in the presence of 0.004 or 0.1 mM Ca^{2+}. Autophosphorylated CaMKIIα was detected with phospho-specific antibody against Thr^{286}, whose phosphorylation is an indicator of CaMKIIα activation (49). CaMKIIα became activated by incubation with WT-CaM in the presence of Ca^{2+} (Fig. 5, *D*–*G*). Remarkably, p-CaMKIIα was significantly increased by Ac-3K-CaM (Fig. 5,

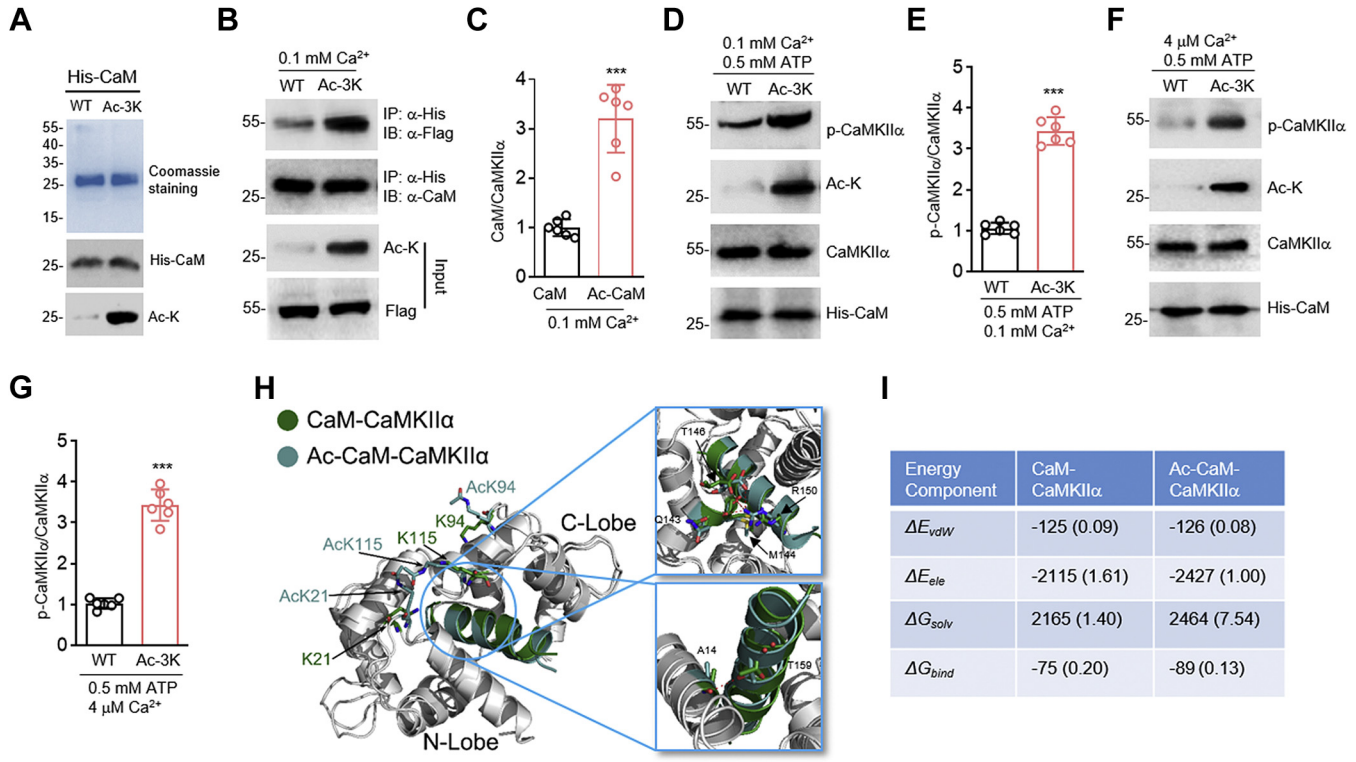

Energy Component	CaM-CaMKIIα	Ac-CaM-CaMKIIα
ΔE_{vdW}	-125 (0.09)	-126 (0.08)
ΔE_{ele}	-2115 (1.61)	-2427 (1.00)
ΔG_{solv}	2165 (1.40)	2464 (7.54)
ΔG_{bind}	-75 (0.20)	-89 (0.13)

Figure 5. Promotion of CaMKIIα activity by acetylated CaM. *A*, purification of His-tagged WT and acetylated CaM proteins from bacteria. *Top*, Coomassie blue staining of 10 μg His-tagged WT and acetylated CaM proteins, *bottom*, western blot of the purified proteins with the indicated Abs. *B*, increased CaMKIIα interaction by acetylated CaM. Flag-CaMKIIα was purified from HEK293 cells and was incubated with His-tagged WT or acetylated CaM to test the interaction in the presence of 0.1 mM Ca^{2+}. CaM was immunoprecipitated with anti-His antibodies and then immunoblotted with anti-Flag antibodies. *C*, quantification of the interaction between WT or acetylated CaM and CaMKIIα in panel *B*. Data were represented as mean ± SD. ***$p < 0.0001$, *t* test, n = 6, data were normalized to WT-CaM. *D*, enhanced CaMKIIα activity by acetylated CaM. Purified Flag-CaMKIIα and His-tagged WT or acetylated CaM were incubated in the presence of 0.1 mM Ca^{2+}. CaMKIIα activity was revealed by anti-p-CaMKIIα. *E*, quantification of p-CaMKIIα/CaMKIIα in panel *D*. Data were represented as mean ± SD. ***$p < 0.0001$, *t* test, n = 6, data were normalized to WT-CaM. *F*, p-CaMKIIα was significantly increased by Ac-3K-CaM compared with WT-CaM in the presence of 4 μM Ca^{2+}. Assay was done as in panel *D*, but in the presence of 4 μM Ca^{2+}. *G*, quantification of p-CaMKIIα/CaMKIIα in panel *F*. Data were represented as mean ± SD. ***$p < 0.0001$, *t* test, n = 6, data were normalized to WT-CaM. *H*, structural comparison of the dominant conformations in CaM-CaMKIIα and Ac-CaM-CaMKIIα simulation system (adopted from PDB code 1CM4). CaM is colored in *gray*. Target peptide from CaMKIIα interacted with CaM and Ac-CaM, which are displayed in *green* and *blue*, respectively. Acetylated residues K21, K94, and K115 are highlighted with *sticks*. *I*, free energy (kcal/mol) analysis for the interaction between WT or acetylated CaM and C18 from CaMKIIα. Data were presented as mean (SEM). ΔE_{ele}, energy contribution from electrostatic force; ΔE_{vdW}, energy contribution from van der Waals force; ΔG_{bind}, total energy change for the protein–protein interaction process; ΔG_{solv}, energy contribution from total solvation-free energy.

D–*G*), suggesting that CaM acetylation promotes CaMKIIα activation. Taken together, these results suggest that acetylated CaM increases the kinase activity of CaMKIIα, compared with WT-CaM.

In the following experiment, we study how acetylation of CaM promotes its interaction with CaMKIIα. Analysis of a 3-D CaM-CaMKIIα complex (Protein Data Bank, ID: 1CM4) from two simulation trajectories suggests that acetylation may increase the flexibility of CaM, enabling a tighter wrapping around CaMKIIα (Fig. 5*H*). Three lysine residues adopted different conformations after acetylation. K21 and K115 (no counting the first methionine) underwent structural reorientations and projected above the binding groove of CaMKIIα. Given their close proximity and favorable topology, K21 and K115 might be closely implicated in the protein–protein interaction. As for K94, allosteric effects might be involved in its impact on the CaM-CaMKIIα interaction upon acetylation, given its relatively distal location to the binding pocket. To further study the impact of CaM acetylation on its interaction with CaMKIIα, we analyzed the free energy ($\Delta G_{binding}$) of the CaM-CaMKIIα interaction by using Amber package (51). The $\Delta G_{binding}$ was calculated by molecular dynamics (MD) simulation of the CaM-CaMKIIα complex (see Experimental procedures). As shown in Figure 5*I*, upon acetylation of CaM, $\Delta G_{binding}$ for CaMKIIα toward CaM decreased from −75 ± 0.2 kcal/mol to −89 ± 0.13 kcal/mol, rendering the binding event more favorable. $\Delta G_{binding}$ is regulated by three parameters—ΔE_{vdW} (van der Waals force), ΔE_{ele} (electrostatic force), and ΔG_{solv} (solvation-free energy). Our result revealed a reduced ΔE_{ele} by CaM acetylation, suggesting a role of the electrostatic force in promoting the CaM-CaMKIIα interaction (Fig. 5*I*).

Generation and characterization of 3KR-Cam1 knockin mice

The K to R mutation is commonly used as a dominant negative mutant for protein acetylation because R preserves the positive charge on the side chain (similar to K), but cannot be acetylated (41, 52). To investigate whether acetylation of CaM on the three lysine residues is important for LTP, we used CRISPR-Cas9 technique to generate mutant

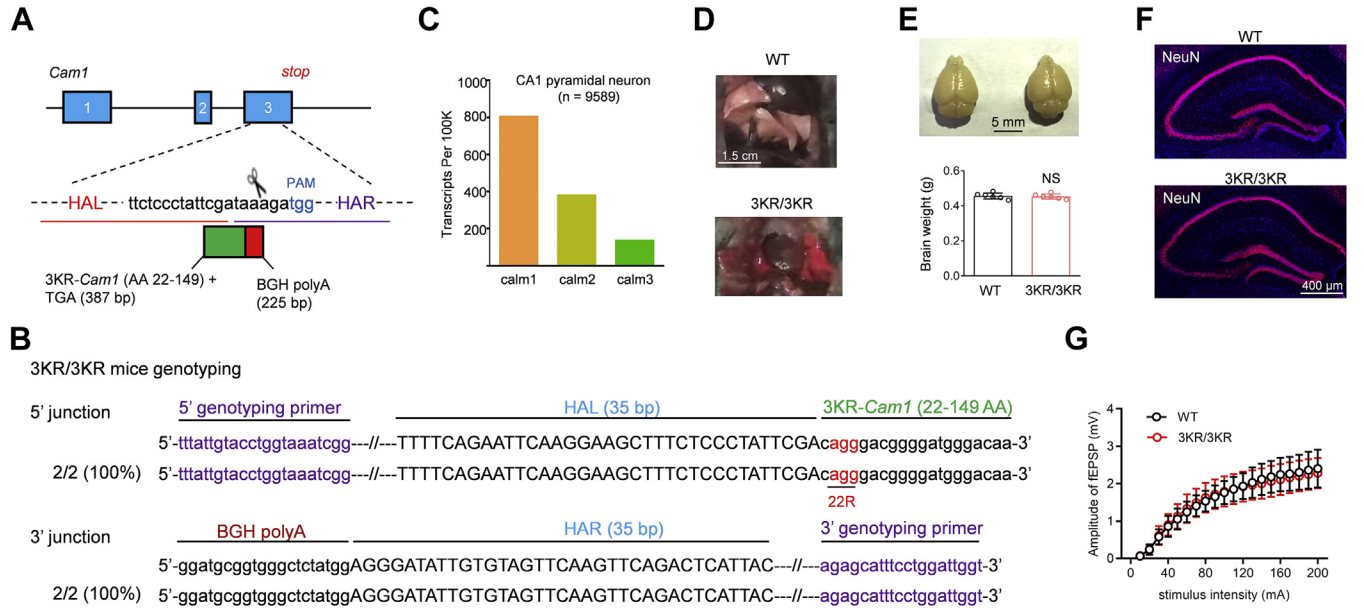

Figure 6. Generation and characterization of 3KR-*Cam1* knockin mice. *A*, schematic overview of generating 3KR-*Cam1* knockin mice using Tild-CRISPR. The knockin fragment was composed of the DNA encoding the 22 to 149 amino acid of 3KR-CaM (*green box*) and the BGH polyA (*red box*) together with the homology arms. The knockin fragment was inserted in exon 3 of mouse *Cam1* gene. HAL or HAR, left or right homology arm. *B*, sequence analysis of 3KR-*Cam1* knockin mice. DNA of mouse tails from 3KR-*Cam1* mouse was isolated. PCR products amplified from 5′ and 3′ junction sites were sequenced. *C*, transcriptional levels of *Cam1* are higher than those of *Cam2* and *Cam3* in CA1 pyramidal neurons of mouse hippocampus (n = 9589 cells). Shown are transcripts of *Cam* genes per 100k total transcripts from single-cell RNA sequencing. *D*, lung hemorrhage in 6-week-old 3KR/3KR mice. *E*, normal brain weight from 5-week-old 3KR/3KR mice. Scale bar, 5 mm. Data were represented as mean ± SD. NS, not significant, *t* test, n = 6. *Top*, representative brain images. *F*, normal global morphology of hippocampus for 5-week-old 3KR/3KR mice. The hippocampal slices were stained with anti-NeuN and DAPI. Scale bar, 400 μm. *G*, similar input–output (I/O) curve at SC-CA1 synapses between WT and 3KR/3KR mice. Data were represented as mean ± SD. F (1,23) = 0.0266, p = 0.8719, two-way ANOVA, n = 13 slices from four WT mice, n = 12 slices from four 3KR/3KR mice.

mice in which K22, 95, and 116 of CaM1 were mutated to R (*i.e.*, 3KR-*Cam1* knockin mice) (Fig. 6, *A* and *B*). Mice have three *Cam* genes—*Cam1*, *Cam2*, and *Cam3*—that encode completely identical proteins, in addition to more distantly related genes (53). Such genetic complexity hinders genetic targeting for all *Cam* genes at the same time. Here we generated 3KR mutant in *Cam1* gene, a dominant isoform whose transcription level is higher than that of *Cam2* and *Cam3* in CA1 pyramidal neurons of mouse hippocampus (http://dropviz.org) (54) (Fig. 6*C*). Since homozygous 3KR-*Cam1* (3KR/3KR) mice died around 6-week-old due to lung hemorrhage (Fig. 6*D*), we used 5-week-old 3KR/3KR mice in the following studies. The brain weight and global morphology of hippocampus were similar between 5-week-old 3KR/3KR and WT mice (Fig. 6, *E* and *F*). Basal glutamatergic transmission such as input–output curve (I/O) at SC-CA1 synapses was not altered in 3KR/3KR mice (Fig. 6*G*).

Importance of CaM acetylation in hippocampal LTP

Hippocampal slices from WT and 3KR/3KR mice were subjected to cLTP stimulation. Autophosphorylated CaMKIIα was detected with phospho-specific antibody against Thr^{286}, whose phosphorylation is an indicator of CaMKIIα activation (49). As shown in Figure 7, *A*–*C*, cLTP-induced CaM acetylation and CaMKIIα activation was diminished in hippocampal slices from 3KR/3KR mice, compared with WT littermates. Note that Ac-CaM was not abolished in 3KR/3KR mice probably because of the intact of *Cam2* and *Cam3* genes. CaMKIIα could phosphorylate the AMPA receptor subunit GluR1 at Ser^{831} during LTP (55, 56). Consistent with the reduction of CaMKIIα activity, p-GluR1 Ser^{831} also decreased in during cLTP in 3KR/3KR mice (Fig. 7, *A* and *D*). These results suggest that acetylation of CaM is important for calcium signaling activated by cLTP stimulation.

We further study whether acetylation of CaM is important for LTP. We performed field potential recording in hippocampal slices from 5-week-old WT and 3KR/3KR mice (Fig. 7*E*). The glutamate release reflected by the paired pulse facilitation (PPF) at SC-CA1 synapses was not altered in 3KR/3KR mice (Fig. 7*F*). However, LTP at SC-CA1 synapses in response to theta burst stimulation (TBS) was greatly attenuated in 3KR/3KR mice, compared with WT littermates (Fig. 7, *G* and *H*). To exclude any potential developmental effects mediated by 3KR/3KR mutant, we studied whether acute delivery of 3KR-CaM recombinant proteins in WT mice could impair LTP. To this end, we purified GST-tagged WT, 3KR, or 3KQ-CaM (mimic acetylation) proteins from bacteria (Fig. 7*I*). The GST-tagged CaM proteins were delivered into hippocampal CA1 neurons through recording peptide, and 30 min later, the high-frequency stimulation (HFS)-induced LTP was recorded (Fig. 7*J*). As indicated in Figure 7, *K* and *L*, 3KR-CaM but not 3KQ-CaM inhibited LTP in hippocampal CA1 neurons from whole-cell recording. Altogether, these results demonstrate an important role of CaM acetylation in LTP.

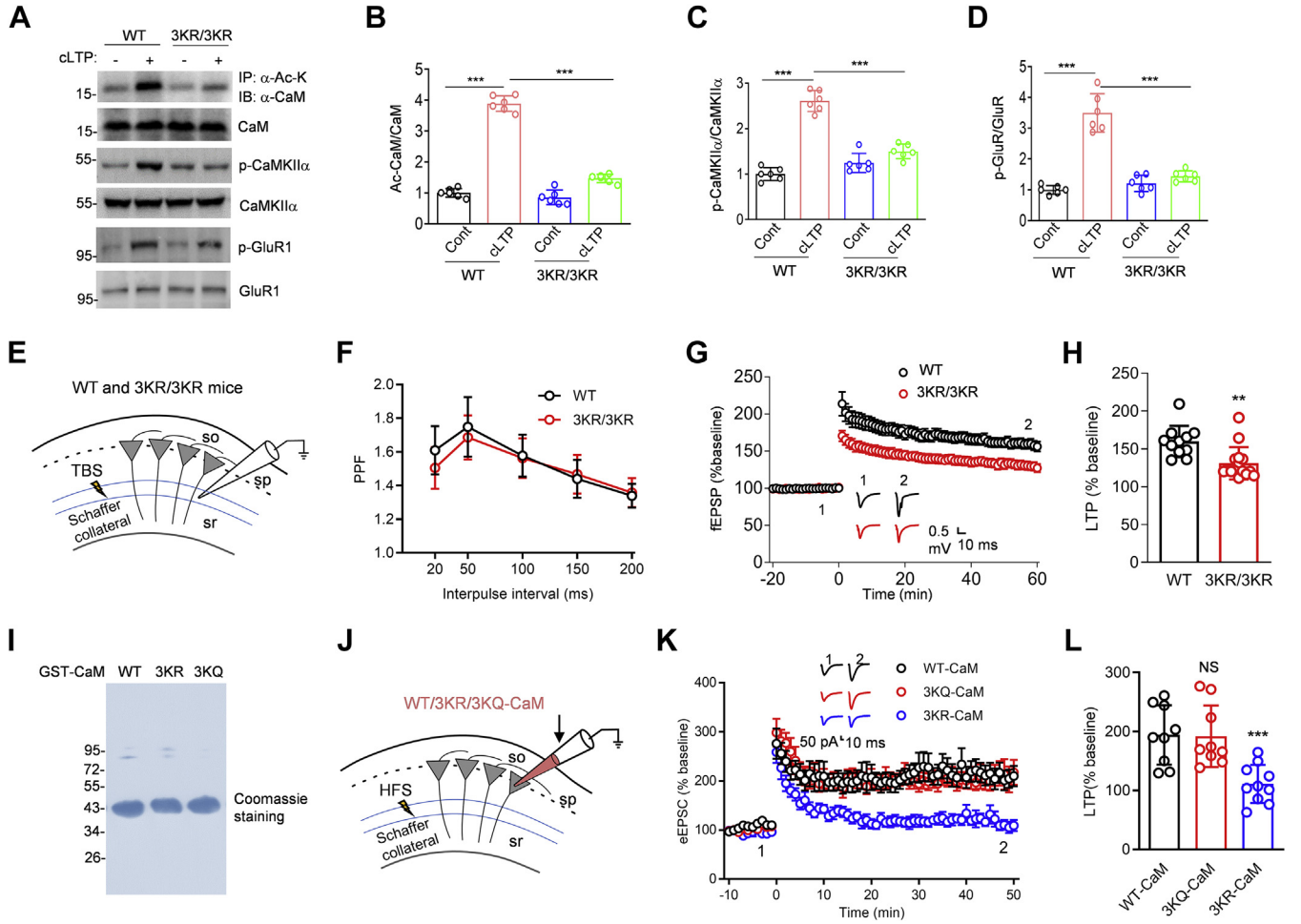

Figure 7. Importance of CaM acetylation in hippocampal LTP. *A*, reduced Ac-CaM, p-CaMKIIα, and p-GluR1 in 3KR/3KR hippocampal slices, in response to cLTP stimulation. *B–D*, quantification of Ac-CaM/CaM (*B*), p-CaMKIIα/CaMKIIα (*C*), and p-GluR1/GluR1 (*D*) in panel *A*. Data were represented as mean ± SD. ***$p < 0.0001$, two-way ANOVA followed by Tukey's multiple comparisons test, n = 6, data were normalized to WT slices under control condition. *E*, diagram showing field EPSP recording at SC-CA1 synapses from WT and 3KR/3KR mice. *F*, comparable paired pulse facilitation (PPF) at SC-CA1 synapses between WT and 3KR/3KR mice. Data were represented as mean ± SD. F (1,19) = 0.304, $p = 0.5876$, two-way ANOVA, n = 10 slices from four WT, n = 11 slices from four 3KR/3KR mice. *G*, normalized fEPSP amplitudes were plotted every 1 min for hippocampal slices from WT and 3KR/3KR mice. *H*, reduced TBS-induced LTP at SC-CA1 synapses in 3KR/3KR hippocampal slices, compared with WT. Data in panel *G* were quantified. Data were represented as mean ± SD. ** $p = 0.0021$, *t* test, n = 11 slices from six WT mice, n = 15 slices from eight 3KR/3KR mice. *I*, Coomassie blue staining of 10 μg GST-tagged WT, 3KR, and 3KQ-CaM proteins purified from bacteria. *J*, diagram showing whole-cell recording of eEPSC in hippocampal CA1 pyramidal neurons. Recording pipettes were infused with GST-WT, 3KR, or 3KQ-CaM. *K*, normalized eEPSC amplitudes were plotted every 1 min for CA1 pyramidal neurons infused with 100 nM GST-WT, 3KR, or 3KQ-CaM. *L*, quantification of LTP in panel K. Data were represented as mean ± SD. NS, not significant, ***$p = 0.001$, one-way ANOVA, n = 9 cells from nine mice for WT and 3KQ-CaM, n = 10 cells from ten mice for 3KR-CaM.

Importance of CaM acetylation in contextual fear learning

The LTP of SC-CA1 synapses is coupled to contextual fear learning (57, 58), which could increase CaM acetylation in the hippocampus (Fig. 3, *L–O*). Lastly, we study whether CaM acetylation plays an important role in contextual fear learning. Because 3KR/3KR mice died prematurely prior to adulthood, due to lung hemorrhage (Fig. 6*D*), we took a knockdown-plus-rescue strategy in adult mice for the behavioral study (Fig. 8*A*). Endogenous CaM was down-regulated by lentivirus expressing shRNAs against *Cam1*, *2*, and *3*, and at the same time, the shRNA-resistant WT-CaM, 3KR-CaM, or 3KQ-CaM was expressed in the hippocampus (Fig. 8, *B–D*). No difference was observed in locomotor activity in open fields among these different groups (Fig. 8, *E* and *F*). Two weeks after injection of lentivirus into hippocampus, mice were subjected to contextual fear training and tests (Fig. 8*G*). In mice where CaM1, 2, and 3 were knocked down and WT-CaM was expressed (*i.e.*, CaMkd+WT-CaM), freezing was normal in exploring, training as well as tests, compared with untreated controls (Fig. 8*H*). In mice where CaM1, 2, and 3 were knocked down and 3KR-CaM was expressed (*i.e.*, CaMkd+3KR-CaM), freezing was normal in exploring and training (Fig. 8*H*). However, their freezing during tests was reduced, compared with controls (Fig. 8*H*), suggesting that CaM acetylation is important for contextual fear learning. On the other hand, CaMkd+3KQ-CaM mice displayed freezing similar to that of control or CaMkd+WT-CaM mice (Fig. 8*H*). These results provide evidence that CaM acetylation is important for contextual fear learning.

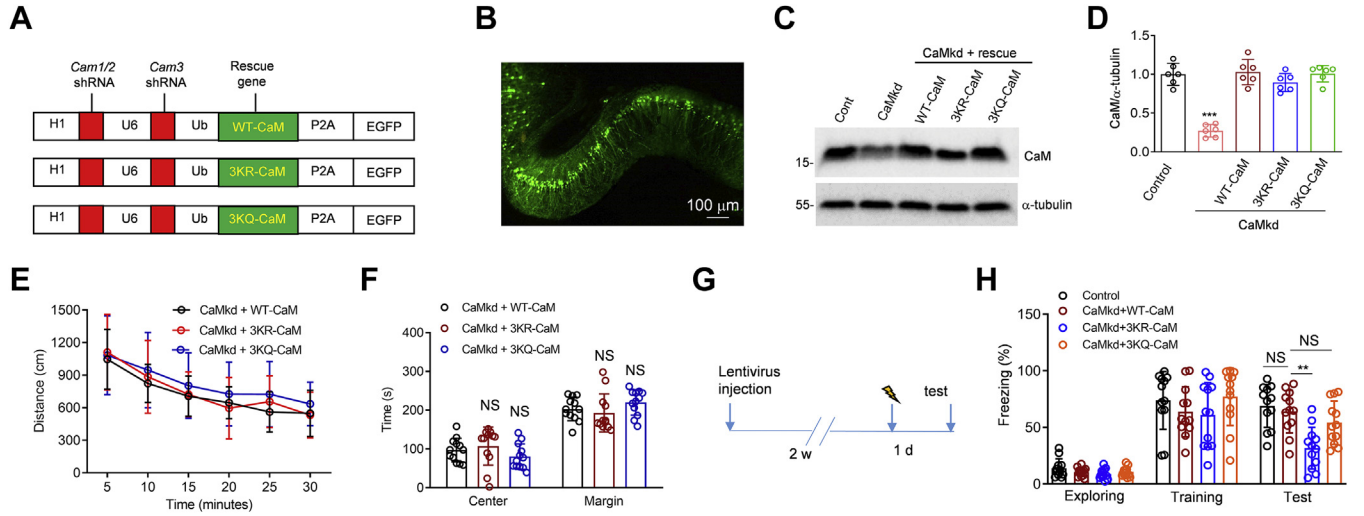

Figure 8. Importance of CaM acetylation in contextual fear learning. *A*, diagram of lentiviral vectors harboring the human H1 and U6 promoters, which drive expression of *Cam1* and *Cam2* shRNA (H1) and *Cam3* shRNA (U6). The vector also contains a ubiquitin promoter (Ub) that drives expression of shRNA-resistant WT, 3KR, or 3KQ-CaM-P2A-EGFP. *B*, expression of EGFP in the hippocampal CA1 region when infected by the lentivirus expressing *Cam1*, *2*, *3* shRNA and WT-CaM and EGFP. Bar, 100 μm. *C*, decreased CaM protein levels by CaMkd lentivirus. The total lysate from DIV 14 mouse hippocampal neurons infected by the indicated lentivirus was probed with indicated Abs. Cont: control virus expressing EGFP, CaMkd, CaM knockdown. *D*, quantification of CaM/α-tubulin in panel *C*. Data were represented as mean ± SD, ***$p < 0.0001$, compared with control, one-way ANOVA, n = 6, data were normalized to control. *E*, equal distance traveled during the first 30 min in open field for mice treated with receiving hippocampal injection of lentivirus. Data were represented as mean ± SD. F (2,33) = 0.6682, $p = 0.5194$, two-way ANOVA, n = 12 mice for each group. *F*, similar time staying in the center and margin of the open field during the first 5 min for mice treated with receiving hippocampal injection of lentivirus. Data were represented as mean ± SD. NS, not significant, compared with CaMKd+WT-CaM, two-way ANOVA followed by Sidak's multiple comparisons test, n = 12 mice for each group. *G*, schematic diagram of behavioral tests. *H*, reduced freezing during paired tests by 3KR-CaM in CaM knockdown mice. Hippocampus was injected with lentivirus expressing 1) shRNA against *Cam1–3*, 2) shRNA-resistant WT-, 3KR, or 3KQ-CaM, and 3) EGFP. Data were represented as mean ± SD. NS, not significant, *$p = 0.0297$, two-way ANOVA followed by Sidak's multiple comparisons test, n = 12 mice for each group.

Discussion

In this study, we provide evidence that acetylation of CaM can be regulated by neural activities and is important for synaptic plasticity and fear learning. Acetylation of CaM occurred within minutes of cLTP stimulation in hippocampal slices, in a time course similar to that of CaMKIIα activation during cLTP stimulation in cultured neurons (59). Mutation of the lysine residues to prevent CaM acetylation impairs hippocampal LTP and contextual fear learning. A parsimonious explanation of these results is that CaM acetylation plays a role in regulating synaptic plasticity.

The stoichiometry level (6%–7%) of CaM acetylation in the total lysates of hippocampus was similar to those of *bona fide* acetylated proteins in mammalian cells (60). The calcium elevation during LTP induction is localized to stimulated spines, or a region called calcium nanodomain, which is near the inner mouth of postsynaptic NMDA receptor (21). The data presented here and in the accompanying paper (61) demonstrated that neural activities increased CaM acetylation through an NMDA receptor and calcium-dependent manner. For these reasons, one could speculate that the increased acetylation of CaM during LTP induction mainly occurred in the stimulated spines or calcium nanodomain. Note that 6% to 7% of CaM acetylation in the stimulated neurons was from the total lysates rather than from the stimulated spines or calcium nanodomain. One could argue that the stoichiometry level of CaM acetylation in the stimulated spines or calcium nanodomain might be much higher than that in the total lysates. Future studies are warranted to generate new tools to study CaM acetylation in the stimulated spines or calcium nanodomain.

How neural activities increase CaM acetylation is an intriguing question. Here we showed that neural activities enhance CaM acetylation through NMDAR activation. Identification of the CaM acetyltransferase will be important for understanding how neural activities increase CaM acetylation. Regardless, our results indicate that CaM acetylation is important for the full activation of CaMKIIα and phosphorylation of GluR1 during LTP. In addition to the GluR1 subunit of AMPA receptor, CaMKIIα can interact with and phosphorylate a variety of synaptic proteins, which contribute to synaptic plasticity and learning (62–65). It will be interesting to study whether CaM acetylation regulates phosphorylation of other downstream target proteins of CaMKIIα.

The results presented here addressed the roles of nonhistone protein acetylation in synaptic plasticity. NMDAR-dependent LTP is arguably the most compelling form of synaptic plasticity (4, 20, 66). NMDAR-dependent LTP operates widely in the brain, but is most extensively studied at Schaffer collateral (SC)-CA1 synapses in the hippocampus (4, 20, 66). The LTP at SC-CA1 synapses in the hippocampus is linked with contextual fear memory (57, 58). These are the reasons why we choose hippocampus in this study. In addition to hippocampus, other brain regions such as amygdala and the hippocampus–amygdala circuit can also regulate contextual fear memory (67–69). Likewise, the LTP in the amygdala also plays important roles in fear memory (69, 70). Future studies are required to investigate whether CaM acetylation can

regulate synaptic plasticity in other brain regions besides hippocampus.

Ideally, a loss-of-function approach could be informative for studying CaM acetylation. However, mice have three *Cam* genes—*Cam1*, *Cam2* and *Cam3*—that encode completely identical proteins, in addition to more distantly related genes (53). Such genetic complexity hinders genetic targeting for all *Cam* genes at the same time. Recent study from single-cell RNA sequencing in adult mouse hippocampus revealed that the gene expression levels of *Cam1* were higher than that of *Cam2* and *Cam3* in CA1 pyramidal neurons (54). Due to these reasons, we generated 3KR/3KR mutant in *Cam1* gene to study the roles of CaM acetylation in LTP at SC-CA1 synapses. Nonetheless, acetylation of CaM2 and CaM3 may remain and account for the residual acetylation in the 3KR/3KR mutant mice. In addition to CaM, the recent studies suggest that LTP is also regulated by other Ca^{2+} sensors such as synaptotagmins (5), which might explain why LTP is not completely abolished in 3KR/3KR mice. K to Q mutation is commonly used to be a mimic of acetyllysine (41, 48), and thus 3KQ-CaM displayed potent activity to stimulate CaMKIIα. However, the CaM acetylation is already very high after cLTP stimulation, which might explain why 3KQ-CaM could not further increase LTP.

CaM, as a calcium sensor, regulates synaptic plasticity by activating kinases such as CaMKIIα and phosphatases including CaN. We provided evidence that acetylated CaM promotes the interaction and activation of CaMKIIα, but not CaN, compared with WT-CaM. In addition to CaMKIIα and CaN, CaM has many other target proteins, several of which have been implicated in synaptic plasticity, neurotransmission, or neuronal excitability (14). For example, CaM regulates NR1 subunit (15), L-type calcium channel (16), cGMP-gated cation channel (71), and other ion channels (17). We observed lung hemorrhage in the 3KR/3KR mice. It might be possible that CaM acetylation affected the interaction and/or function of proteins critical for the integrity of endothelial cells in the pulmonary blood vessels. Future work is warranted to investigate whether CaM acetylation alters the function of these proteins.

Experimental procedures

Animals

C57BL/6N male mice at age of 7 to 8 weeks were used in experiments unless otherwise described. Animals were housed in rooms at 23 °C and 50% humidity in a 12 h light/dark cycle and with food and water available *ad libitum*. All experimental procedures were approved by the Institutional Animal Care and Use Committees of East China Normal University.

K22, 95, 116R (3KR) knockin mice were generated on C57BL/6 background using Tild-CRISPR (targeted integration with linearized dsDNA-CRISPR) (72). The Tild donor vector for 3KR-*Cam1* contained 35 bp HAL-3KR-Cam1(22–149 amino acid)-BGH polyA-35 bp HAR. The exon3 of mouse *Cam1* gene was replaced by the Tild donor vector. Two gRNAs targeting *Cam1* exon 3 (sgRNA-L: ttctccctattcgataaagatgg, sgRNA-R: ttagaactgagtgagcaccaggg) were transcribed *in vitro*. A mixture of Cas9 mRNA (100 ng/ml), sgRNAs (50 ng/ml), and donor vectors (50 ng/ml) was injected into fertilized eggs. A total of 694 injected zygotes were transferred into recipients, and 124 pups were obtained and genotyped. The PCR amplification of the targeting loci and DNA sequencing validated the correct gene targeting. The 3KR-*Cam1* founder mouse was crossed with WT C57BL/6 mice for three generations, and the F4 homozygous 3KR-*Cam1* knockin (3KR/3KR) mice were used for experiments. Since most 3KR/3KR mice died at 6 weeks old due to the lung hemorrhage, 5-week-old 3KR/3KR male mice were used in LTP experiments. The genotyping primers for WT and 3KR-*Cam1* knockin mice are as follows: forward: 5′TTTAT TGTAC CTGGT AAATC GG 3′, reverse: 5′ACCAA TCCAG GAAAT GCTCT 3′. The genotyping products for WT and 3KR-*Cam1* are 646 and 1115 bp, respectively.

Western blot

Homogenates of hippocampal tissue were prepared in RIPA buffer containing 50 mM Tris–HCl, pH 7.4, 150 mM NaCl, 2 mM EDTA, 1% sodium deoxycholate, 1% Triton X-00, 1 mM PMSF, 50 mM sodium fluoride, 1 mM sodium vanadate, 1 mM DTT, and protease inhibitors cocktails. PSD fractions were directly dissolved in 1× SDS-PAGE sample buffer. All the protein samples were boiled in 100 °C water bath for 10 min before western blot. The homogenates were resolved on SDS-PAGE and transferred to nitrocellulose membranes, which were incubated in the TBS buffer containing 0.1% Tween-20 and 5% milk for 1 h at room temperature before incubation with a primary antibody overnight at 4 °C. After wash, the membranes were incubated with an HRP-conjugated secondary antibody in the same TBS buffer for 1 h at room temperature. Immunoreactive bands were visualized by ChemiDocTM XRS + Imaging System (BIO-RAD) using enhanced chemiluminescence (Pierce) and analyzed with Image J (NIH). The primary antibodies used were as follows: anti-Histone H3, Cell Signaling (9715); anti-Calmodulin, Millipore (05-173); anti-CaMKIIα, Cell Signaling (11945); anti-p-CaMKIIα Thr^{286}, Sigma (SAB4300228); anti-Acetyllysine, Cell Signaling (9441); anti-p-GluR1 Ser^{831}, Abcam (ab109464); anti-GluR1, Abcam (ab109450); anti-GST, Abmart (12G8); and anti-His, Abmart (10E2).

Detection of CaM acetylation

Because the CaM monoclonal antibody was not suitable for IP, we opted to purify acetylated proteins. Lysates were incubated with acetyllysine antibody-conjugated agarose (ImmuneChem, ICP0388) on a rotor shaker at 4 °C overnight. After incubation, agarose heads were washed with PBST four times through repeating centrifugation and aspiration. Sixty microliter 2× SDS-PAGE loading buffer without DTT or 2-mercaptoethanol was added to the beads, vortexed, and boiled for 5 min. After centrifuging the beads at 5000 rpm for 2 min, the supernatant was used for western blot with mouse anti-CaM antibodies. To generate site-specific anti-acetylated CaM antibodies against K22, 95, or 116, rabbits were

immunized with 500 μg of peptides C-FSLFD(Ac-K)DGDGT, C-FRVFD(Ac-K)DGNGY and C-TNLGE(Ac-K)LTDEE with complete Freund's adjuvant three times, and boosted with 250 μg peptides with incomplete Freund's adjuvant additional four times. Rabbit anti-serum was collected and purified by respective nonacetylated peptides.

Subcellular fractions

Mouse brain tissues were homogenized in Buffer A (0.32 M sucrose, 1 mM $MgCl_2$, 1 mM PMSF and a protease inhibitor cocktail). Homogenates were passed through a filter to remove cell debris and centrifuged at 500*g* for 5 min in a fixed angle rotor to yield P1 and S1 fractions. P1 fractions were washed in Buffer B containing 10 mM KCl, 1.5 mM $MgCl_2$, 10 mM Tris-HCl (pH 7.4) and centrifuged at 500*g* for 5 min. Pellets were dissolved in Buffer C containing 20 mM HEPES (pH 7.9), 25% glycerol, 1.5 mM $MgCl_2$, 1.4 M KCl, 0.2 mM EDTA, 0.2 mM PMSF, 0.5 mM DTT and incubated on a shaker at 4 °C for 30 min. After centrifugation at 12,000*g* for 10 min, the supernatant of P1 was collected as nuclear proteins. The S1 fraction was centrifuged at 10,000*g* for 10 min to yield P2 that contains membranes and synaptosomes and the cytoplasmic S2.

P2 fractions were resuspended in 0.32 M sucrose, which was then layered onto 0.8 M sucrose. After being centrifuged at 9100*g* for 15 min in a swinging bucket rotor, synaptosomes were collected from 0.8 M sucrose layer and concentrated by centrifugation at 20,800*g* for 1 h. To further purify the postsynaptic (PSD) fractions, synaptosomes in the 0.8 M sucrose solution were mixed with 1/19 volume of Buffer D containing 200 mM HEPES (pH 7.0), 20% Triton X-100, and 1.5 M KCl. Samples were centrifuged at 20,800*g* for 45 min using a fixed angle rotor. The resulting pellets were resuspended in Buffer E containing 1% Triton X-100 and 75 mM KCl using a Dounce mini-homogenizer and centrifuged again at 20,800*g* for 30 min to yield final pellets (PSD fraction), which were washed with 20 mM HEPES (pH 7.9) and dissolved in 1× SDS-PAGE sample buffer.

Chemical LTP and LTD

cLTP stimulation in hippocampal slices was performed as previously described (43). Briefly, cLTP was induced by incubating slices for 15 min in aCSF lacking $MgCl_2$ and containing 4 mM $CaCl_2$, 100 μM picrotoxin, 50 μM forskolin, and 100 nM rolipram. For western blots, the brain slices were collected 1 or 10 min after cLTP stimulation. cLTD in hippocampal slices was induced by submerging the slices in 30 μM NMDA for 3 min, as previously described (73). Slices were transferred to a well containing standard aCSF solution.

Immunofluorescence

Brain slices were fixed in 4% PFA, permeabilized with 0.3% Triton-X 100 and 5% BSA in PBS, and incubated with primary antibodies at 4 °C overnight. After washing with PBS for three times, samples were incubated with Alexa Fluor-594 secondary antibodies (1:1000, Invitrogen) for 1 h at room temperature. Samples were mounted with Vectashield mounting medium (Vector) and images were taken by Leica TCS SP8 confocal microscope. The following primary antibody was used: rabbit anti-NeuN (Abcam, ab177487).

Purification of site-specifically acetylated CaM recombinant proteins

The site-specifically acetylated CaM recombinant proteins were synthesized according to a previous report (47). In brief, *Escherichia coli* strain, BL21 (DE3), was transformed with plasmids pAcKRS-3 and pCDF PylT-1 carrying the ORF for Cam with an amber codon at the desired site. The cells were first grown overnight in LB medium supplemented with 50 mg/ml kanamycin and 50 mg/ml spectinomycin (LB-KS) at 37 °C. Two-milliliter bacteria were cultured overnight and then inoculated into 200 ml LB-KS for further culturing. When the OD600 reached 0.4∼0.6, 20 mM nicotinamide (NAM) and 10 mM acetyl-lysine were added, and 30 min later, the protein expression was induced at 18 °C overnight by adding 0.5 mM IPTG. Cells were harvested after induction and were washed with ice-cold PBS containing 20 mM NAM, the proteins were purified with HisTrap FF (GE Healthcare, 17-5319-01) according to the manufacturer's protocol.

Stoichiometry of CaM acetylation at K22, 95, and 116

We used purified acetylated CaM proteins as standards to analyze the stoichiometry levels for each acetylated lysine residue of CaM under control and cLTP conditions. The standard samples containing 0%, 0.1%, 0.3%, 1%, 3%, and 10% acetylated His-CaM proteins in 1 μg total His-CaM proteins were subjected to ELISA assay in 96-well microplates, which were coated with 100 μl site-specific anti-Ac-CaM antibodies (0.01 μg/ml) overnight. The hippocampal lysates with 100 μg proteins were used for the same ELISA assay considering that the endogenous CaM proteins were about 1% of total proteins in the hippocampus (74). The standard samples and hippocampal lysates with the volume of 100 μl were added to each well and were incubated for 2 h at room temperature, and then each well was washed with PBS containing 0.1% Tween-20 for three times. After washing, 100 μl secondary antibodies (HRP-conjugated goat-anti-rabbit IgG, 1 μg/ml) was added to each well and incubated for 2 h at room temperature. After that, each well was washed with PBS containing 0.1% Tween-20 for three times before adding 100 μl HRP substrate solution (1:1 mixture of Color Reagent A H_2O_2 and Color Reagent B Tetramethylbenzidine, R&D Systems, Catalog # DY999) into each well. After incubation with the HRP substrate solution for 20 min at room temperature, 50 μl of stop solution (2 N H_2SO_4, R&D Systems, Catalog # DY994) was applied to each well. The optical density of each well was determined using a microplate reader set to 450 nm. We first generated a standard curve for stoichiometry of standard samples containing different concentration of Ac-CaM and then determined the stoichiometry levels of endogenous Ac-CaM proteins in the hippocampal lysates.

GST pull-down

GST-tagged WT-CaM or CaM with K to R mutation was expressed in *E. coli* BL21 cells and purified using Glutathione Sepharose 4 Fast Flow (GE Health) according to the manufacturer's instructions. His-tagged CaMKIIα and acetylated CaM proteins were purified using Ni-NTA agarose beads (QIAGEN) following the manufacturer's protocols. For binding assays, purified His-CaMKIIα proteins (1 μM) were incubated with immobilized GST-CaM (1 μM) for 2 h at 4 °C with 1 mM EGTA (no Ca^{2+}, as a negative control), 0.1 mM, or 1 mM $CaCl_2$. The mixture was then washed, eluted, and subjected to western blot with anti-His and anti-GST antibodies (Abmart).

In vitro *CaMKIIa autophosphorylation*

In brief, the purified His-CaMKIIα proteins (1 μM) and GST-tagged WT, 3KR, or 3KQ-CaM proteins (1 μM) were incubated at 31 °C for 5 min in the reaction buffer (500 μM ATP, 50 mM HEPES, pH 7.5, 1 mM DTT, 0.1% Tween-20, and 10 mM $MgCl_2$) with 1 mM EGTA (no Ca^{2+}, as a negative control), 0.1 mM, or 4 μM $CaCl_2$ with constant shaking. Reactions were stopped by an addition of 2× SDS sampling buffer, followed by western blot with anti-p-CaMKIIαThr^{286} (Sigma, SAB4300228) and anti-CaMKIIα antibodies (Cell Signaling, 11945).

Calcineurin activity assay

The phosphatase activity of calcineurin was assayed by a colorimetric kit (Abcam, ab139461) according to the manufacturer's instructions. The kit provided both the A and B subunit of calcineurin. Dephosphorylation of the RII phosphopeptide substrate in the presence of CaM was detected by the green assay. Optical density OD 620 nm, which indicates the phosphatase activity, was read on a microplate reader (Thermo Fisher Scientific).

BRET assay

We applied bioluminescence resonance energy transfer (BRET) assay (50) to study CaM-CaMKIIα interaction in HEK293 cells. We first transfected one dish (10 cm diameter) of cells with 10 mg BRET plasmids containing WT, 3KR, or 3KQ-Cam and the target peptide from CaMKIIα (C18). The cells were harvested with 10 ml KCl (100 mM) 48 h after transfection and were separated into ten 15 ml centrifuge tubes. After spin-down (500 rpm × 5 min), the pellet was resuspended with calcium calibration buffer (Invitrogen, C-3008MP) plus 1000 units/ml α-hemolysin (Sigma, H9395). We added 200 μl cell resuspension solution plus 50 μl luciferase substrate (Promega, S2011) in each well of 96-well plate and then read the emission ratio of 530 nm to 480 nm. The calcium concentration was adjusted to 0, 0.1, 0.3, 1, 3, 10, 30, 100 μM for Ca^{2+} binding assay using the calcium calibration buffer kit. A Ca^{2+} titration curve was used to calculate Kd value by nonlinear regression analysis. The averaged data from four independent experiments were fitted to the Hill equation using Prism 8 software.

Molecular dynamics simulation

We carried out 200 ns MD simulation for CaM-CaMKIIα interaction systems in the presence or absence of acetylation with the help of Amber package(51). The CaM-CaMKIIα complex structure was extracted from Protein Data Bank (PDB ID: 1CM4), and for the acetylated system, modifications were introduced and optimized through Discovery Studio. After setting up, Amber ff14SB force field was applied to the parameter calculations and TIP3P water model was used for the system solvation. NaCl ions were added to the complex systems for the charge neutralization and the simulation of the physiological conditions. After the primary preparations, two rounds of energy minimization were carried out. In the first step, the overall structural scaffolds were held rigid and water and counterions underwent a 5000-step maximum minimization cycles. After that, the whole systems were relaxed, and minimizations with no restriction followed. Then, under NVT conditions, two simulation systems were heated up from 0 to 300 K within 300 ps. They were further equilibrated at 300 K for another 700 ps, after which, 200 ns of MD simulations were performed for these two systems respectively. Analyses of the simulation trajectories were carried out with the cpptraj and MMPBSA.py plugin within Amber package. In total, 200 representative snapshots from the last 180 ns trajectories, when the simulations had already reached equilibrium, were extracted for detailed investigations.

For binding free energy evaluation, we followed the Equation 1 below, with the complex systems, the receptors (CaM/acetylated CaM), and the ligands (CaMKIIα) calculated respectively.

$$\Delta G_{binding} = \Delta G_{complex} - \Delta G_{receptor} - \Delta G_{ligand} \quad (1)$$

Within Equation 1, the free energy terms were given by the following Equation 2:

$$\Delta G = \Delta E_{vdW} + \Delta E_{ele} + \Delta G_{solv} \quad (2)$$

in which ΔE_{vdW} denoted the energy contribution from van der Waals force, ΔE_{ele} represented the energy contribution from electrostatic force, and ΔG_{solv} referred to the energy contribution from total solvation-free energy.

LTP recording and quantification

Hippocampal slices from 5-week-old WT and 3KR/3KR mice were placed in a recording chamber continuously superfused with prewarmed (32 °C ± 1 deg. C) aCSF at a rate of 3 ml/min. fEPSPs were evoked (0.033 Hz, 0.1 ms current pulses) in the CA1 stratum radiatum by stimulating Schaffer collateral (SC) with a two-concentric bipolar stimulating electrode (FHC) and recorded in current-clamp by a HEKA EPC 10 (HEKA Elektronik) amplifier with aCSF-filled glass pipettes (1–5 MΩ). LTP was induced using three trains of theta burst stimulation (ten bursts at 5 Hz, each having 50 pulses, at 100 Hz) with intertrain intervals of 30 s (75, 76).

Whole-cell LTP recording was performed as previously described (5). Three-week-old male mice were used for whole-cell LTP recording with 20 μM BIC in the aCSF. Briefly, EPSCs of hippocampal CA1 pyramidal neurons were evoked (0.1 Hz, 0.1 ms current pulses) by stimulating SC with electrode placed 200 μm away from recorded neurons at −70 mV. LTP was induced by three trains of high-frequency stimulation (HFS, 100 Hz, 1 s) separated by 20 s with the patched cells depolarized to −20 mV. To avoid "wash-out" of LTP, the HFS was applied within 10 min after achieving whole cell configuration.

All data were acquired at a 10 kHz sampling rate of using PATCHMASTER version 2 x 90.1 software (HEKA Elektronik) and filtered offline at 2 kHz. Analysis was performed with Neuromatic version 3.0 (http://www.neuromatic.thinkrandom.com). Each EPSP or EPSC trace was normalized to baseline. Two consecutive EPSP or six consecutive EPSC traces were averaged to generate 1-min bin, which generated LTP summary time course graphs. For the LTP of field potential, the magnitude of LTP was calculated at an average of normalized EPSP amplitudes 50 to 60 min after TBS. For whole-cell LTP, the magnitude of LTP was calculated at the averaged of normalized EPSC amplitudes 45 to 50 min after HFS.

Generation and stereotaxic injection of lentivirus (LV)

The lentivirus vectors expressing *Cam* shRNA and rescue genes were kindly provided by Dr Thomas C. Südof (53). We changed the sequence of IRES in the original vector to p2A to increase the expression level of EGFP. All the AAV and lentivirus were generated in OBiO Technology Corp, Ltd. For virus injection, WT male mice at age of 7 to 8 weeks were anesthetized with 1% pentobarbital sodium (100 mg/kg, i.p.) and were placed in a stereotaxic apparatus (RWD Life Science). Viruses were injected bilaterally in the CA1 regions of hippocampus with the coordinates: anteroposterior (AP) −2.7 mm, mediolateral (ML) ± 2.25 mm, dorsoventral (DV) −1.625 mm relative to bregma. Each injection used 1 μl LV and took 10 min. After injection, the glass pipette was left in place for 5 min in order to facilitate diffusion of the virus. The injection sites were examined at the end of the experiments, and animals with incorrect injection site were excluded from the data analysis. Two weeks after LV injection, mice were subjected to experiments. All surgery was conducted with aseptic technique.

Contextual fear conditioning

The investigators who performed behavioral analysis were blind to the genotype or treatment of the mice. Eight-week-old mice were first habituated to the behavioral room and apparatus (Fear Conditioning System, Panlab) for 5 min. During training, mice were placed in the conditioning chamber and exposed to three foot shocks (2 s, 0.5 mA) with an interval of 30 s. One day after training, mice were returned to the chamber to evaluate contextual fear learning. Freezing during training and testing was scored using PACKWIN software. Data were expressed as percent freezing in 180-s epochs, with each epoch divided into 12 bins.

Statistics

All the data were shown as mean ± SD. Comparisons between two groups were made using unpaired *t* test. Comparisons between three or more groups were made using one-way ANOVA analysis followed by Tukey's post-hoc test. Data on the binding curve between CaM and C18, CaM and M13, I/O curve, and PPF at SC-CA1 synapse were analyzed by two-way-ANOVA. Statistically significant difference was indicated as follows: $^{***}p < 0.001$, $^{**}p < 0.01$, and $^{*}p < 0.05$. The statistical analysis was performed with the software of GraphPad Prism 8.

Data availability

All data supporting the results presented herein are available from the article paper.

Supporting information—This article contains supporting information.

Acknowledgments—This work was supported by grants from National Natural Science of China (No. 31970900), the Fundamental Research Funds for the Central Universities, the Program for Professor of Special Appointment (Eastern Scholar) at Shanghai Institutions of Higher Learning. We thank Dr Thomas C. Südhof (Stanford, USA) for providing the lentivirus vectors expressing *Cam* shRNA, Dr Jason W. Chin (Cambridge, UK) for providing the pAcKRS-3 and pCDF PylT-1 plasmids, Dr Takeharu Nagai (Tokyo, Japan) for providing the backbone of the BRET constructs, Dr Nevin A. Lambert (Augusta, USA) for assisting BRET assay, Dr Dali Li (ECNU, China) for help in generating 3KR-*Cam1* knockin mice.

Author contributions—H.-L. Z. and D.-M. Y. conceptualization; H.-L. Z., B. Z., W. H., P. Y., and D.-M. Y. data curation; H.-L. Z., Y.-B. S., and D.-M. Y. formal analysis; D.-M. Y. funding acquisition; H.-L. Z., B. Z., W. H., Y.-B. S., P. Y., Y. C., D. N., and J. Z. investigation; H.-L. Z., B. Z., W. H., P. Y., Y. C., D. N., and J. Z. methodology; H.-L. Z. and D.-M. Y. project administration; D.-M. Y. supervision; H.-L. Z., B. Z., W. H., P. Y., and D.-M. Y. validation; H.-L. Z., B. Z., W. H., and P. Y. visualization; H.-L. Z. and D.-M. Y. writing—original draft; D.-M. Y. writing-review and editing.

Conflict of interest—The authors declare no competing interests.

Abbreviations—The abbreviations used are: CaM, calmodulin; CaMKIIα, calcium/calmodulin-dependent protein kinase IIα; cLTP, chemical LTP; LTP, long-term potentiation; MD, molecular dynamics; NAM, nicotinamide; PPF, paired pulse facilitation; SC, Schaffer collateral.

References

1. Flavell, S. W., and Greenberg, M. E. (2008) Signaling mechanisms linking neuronal activity to gene expression and plasticity of the nervous system. *Annu. Rev. Neurosci.* **31**, 563–590
2. Ma, H., Groth, R. D., Cohen, S. M., Emery, J. F., Li, B., Hoedt, E., Zhang, G., Neubert, T. A., and Tsien, R. W. (2014) gammaCaMKII shuttles

Ca(2)(+)/CaM to the nucleus to trigger CREB phosphorylation and gene expression. *Cell* **159**, 281–294
3. Biever, A., Donlin-Asp, P. G., and Schuman, E. M. (2019) Local translation in neuronal processes. *Curr. Opin. Neurobiol.* **57**, 141–148
4. Huganir, R. L., and Nicoll, R. A. (2013) AMPARs and synaptic plasticity: The last 25 years. *Neuron* **80**, 704–717
5. Wu, D., Bacaj, T., Morishita, W., Goswami, D., Arendt, K. L., Xu, W., Chen, L., Malenka, R. C., and Sudhof, T. C. (2017) Postsynaptic synaptotagmins mediate AMPA receptor exocytosis during LTP. *Nature* **544**, 316–321
6. Shi, S. H., Hayashi, Y., Petralia, R. S., Zaman, S. H., Wenthold, R. J., Svoboda, K., and Malinow, R. (1999) Rapid spine delivery and redistribution of AMPA receptors after synaptic NMDA receptor activation. *Science* **284**, 1811–1816
7. Coba, M. P. (2019) Regulatory mechanisms in postsynaptic phosphorylation networks. *Curr. Opin. Struct. Biol.* **54**, 86–94
8. Soderling, T. R., and Derkach, V. A. (2000) Postsynaptic protein phosphorylation and LTP. *Trends Neurosci.* **23**, 75–80
9. Watterson, D. M., Sharief, F., and Vanaman, T. C. (1980) The complete amino acid sequence of the Ca2+-dependent modulator protein (calmodulin) of bovine brain. *J. Biol. Chem.* **255**, 962–975
10. Schafer, B. W., and Heizmann, C. W. (1996) The S100 family of EF-hand calcium-binding proteins: Functions and pathology. *Trends Biochem. Sci.* **21**, 134–140
11. Brose, N., Petrenko, A. G., Sudhof, T. C., and Jahn, R. (1992) Synaptotagmin: A calcium sensor on the synaptic vesicle surface. *Science* **256**, 1021–1025
12. Berridge, M. J. (1998) Neuronal calcium signaling. *Neuron* **21**, 13–26
13. Ghosh, A., and Greenberg, M. E. (1995) Calcium signaling in neurons: Molecular mechanisms and cellular consequences. *Science* **268**, 239–247
14. Xia, Z., and Storm, D. R. (2005) The role of calmodulin as a signal integrator for synaptic plasticity. *Nat. Rev. Neurosci.* **6**, 267–276
15. Ehlers, M. D., Zhang, S., Bernhadt, J. P., and Huganir, R. L. (1996) Inactivation of NMDA receptors by direct interaction of calmodulin with the NR1 subunit. *Cell* **84**, 745–755
16. Zuhlke, R. D., Pitt, G. S., Deisseroth, K., Tsien, R. W., and Reuter, H. (1999) Calmodulin supports both inactivation and facilitation of L-type calcium channels. *Nature* **399**, 159–162
17. Saimi, Y., and Kung, C. (2002) Calmodulin as an ion channel subunit. *Annu. Rev. Physiol.* **64**, 289–311
18. Kitchen, P., Salman, M. M., Halsey, A. M., Clarke-Bland, C., MacDonald, J. A., Ishida, H., Vogel, H. J., Almutiri, S., Logan, A., Kreida, S., Al-Jubair, T., Winkel Missel, J., Gourdon, P., Tornroth-Horsefield, S., Conner, M. T., *et al.* (2020) Targeting aquaporin-4 subcellular localization to treat central nervous system edema. *Cell* **181**, 784–799.e719
19. Chin, D., and Means, A. R. (2000) Calmodulin: A prototypical calcium sensor. *Trends Cell Biol.* **10**, 322–328
20. Malenka, R. C., and Bear, M. F. (2004) LTP and LTD: An embarrassment of riches. *Neuron* **44**, 5–21
21. Lisman, J., Yasuda, R., and Raghavachari, S. (2012) Mechanisms of CaMKII action in long-term potentiation. *Nat. Rev. Neurosci.* **13**, 169–182
22. Swaminathan, P. D., Purohit, A., Hund, T. J., and Anderson, M. E. (2012) Calmodulin-dependent protein kinase II: Linking heart failure and arrhythmias. *Circ. Res.* **110**, 1661–1677
23. Parra, V., and Rothermel, B. A. (2017) Calcineurin signaling in the heart: The importance of time and place. *J. Mol. Cell. Cardiol.* **103**, 121–136
24. Miyawaki, A., Griesbeck, O., Heim, R., and Tsien, R. Y. (1999) Dynamic and quantitative Ca2+ measurements using improved cameleons. *Proc. Natl. Acad. Sci. U. S. A.* **96**, 2135–2140
25. Allfrey, V. G., Faulkner, R., and Mirsky, A. E. (1964) Acetylation and methylation of histones and their possible role in the regulation of RNA synthesis. *Proc. Natl. Acad. Sci. U. S. A.* **51**, 786–794
26. Shahbazian, M. D., and Grunstein, M. (2007) Functions of site-specific histone acetylation and deacetylation. *Annu. Rev. Biochem.* **76**, 75–100
27. Graff, J., and Tsai, L. H. (2013) Histone acetylation: Molecular mnemonics on the chromatin. *Nat. Rev. Neurosci.* **14**, 97–111
28. Alarcon, J. M., Malleret, G., Touzani, K., Vronskaya, S., Ishii, S., Kandel, E. R., and Barco, A. (2004) Chromatin acetylation, memory, and LTP are impaired in CBP+/- mice: A model for the cognitive deficit in Rubinstein-Taybi syndrome and its amelioration. *Neuron* **42**, 947–959
29. Vecsey, C. G., Hawk, J. D., Lattal, K. M., Stein, J. M., Fabian, S. A., Attner, M. A., Cabrera, S. M., McDonough, C. B., Brindle, P. K., Abel, T., and Wood, M. A. (2007) Histone deacetylase inhibitors enhance memory and synaptic plasticity via CREB: CBP-dependent transcriptional activation. *J. Neurosci.* **27**, 6128–6140
30. Guan, J. S., Haggarty, S. J., Giacometti, E., Dannenberg, J. H., Joseph, N., Gao, J., Nieland, T. J., Zhou, Y., Wang, X., Mazitschek, R., Bradner, J. E., DePinho, R. A., Jaenisch, R., and Tsai, L. H. (2009) HDAC2 negatively regulates memory formation and synaptic plasticity. *Nature* **459**, 55–60
31. Gu, W., and Roeder, R. G. (1997) Activation of p53 sequence-specific DNA binding by acetylation of the p53 C-terminal domain. *Cell* **90**, 595–606
32. Maruta, H., Greer, K., and Rosenbaum, J. L. (1986) The acetylation of alpha-tubulin and its relationship to the assembly and disassembly of microtubules. *J. Cell Biol.* **103**, 571–579
33. Zhao, S., Xu, W., Jiang, W., Yu, W., Lin, Y., Zhang, T., Yao, J., Zhou, L., Zeng, Y., Li, H., Li, Y., Shi, J., An, W., Hancock, S. M., He, F., *et al.* (2010) Regulation of cellular metabolism by protein lysine acetylation. *Science* **327**, 1000–1004
34. Lee, I. H., and Finkel, T. (2009) Regulation of autophagy by the p300 acetyltransferase. *J. Biol. Chem.* **284**, 6322–6328
35. Narita, T., Weinert, B. T., and Choudhary, C. (2019) Functions and mechanisms of non-histone protein acetylation. *Nat. Rev. Mol. Cell Biol.* **20**, 156–174
36. Choudhary, C., Kumar, C., Gnad, F., Nielsen, M. L., Rehman, M., Walther, T. C., Olsen, J. V., and Mann, M. (2009) Lysine acetylation targets protein complexes and co-regulates major cellular functions. *Science* **325**, 834–840
37. Wang, G., Li, S., Gilbert, J., Gritton, H. J., Wang, Z., Li, Z., Han, X., Selkoe, D. J., and Man, H. Y. (2017) Crucial roles for SIRT2 and AMPA receptor acetylation in synaptic plasticity and memory. *Cell Rep.* **20**, 1335–1347
38. Cheung, W. Y. (1980) Calmodulin plays a pivotal role in cellular regulation. *Science* **207**, 19–27
39. Means, A. R., and Dedman, J. R. (1980) Calmodulin–an intracellular calcium receptor. *Nature* **285**, 73–77
40. Klee, C. B., Crouch, T. H., and Richman, P. G. (1980) Calmodulin. *Annu. Rev. Biochem.* **49**, 489–515
41. Kim, S. C., Sprung, R., Chen, Y., Xu, Y., Ball, H., Pei, J., Cheng, T., Kho, Y., Xiao, H., Xiao, L., Grishin, N. V., White, M., Yang, X. J., and Zhao, Y. (2006) Substrate and functional diversity of lysine acetylation revealed by a proteomics survey. *Mol. Cell* **23**, 607–618
42. Lundby, A., Lage, K., Weinert, B. T., Bekker-Jensen, D. B., Secher, A., Skovgaard, T., Kelstrup, C. D., Dmytriyev, A., Choudhary, C., Lundby, C., and Olsen, J. V. (2012) Proteomic analysis of lysine acetylation sites in rat tissues reveals organ specificity and subcellular patterns. *Cell Rep.* **2**, 419–431
43. Otmakhov, N., Khibnik, L., Otmakhova, N., Carpenter, S., Riahi, S., Asrican, B., and Lisman, J. (2004) Forskolin-induced LTP in the CA1 hippocampal region is NMDA receptor dependent. *J. Neurophysiol.* **91**, 1955–1962
44. Quinn, J. J., Loya, F., Ma, Q. D., and Fanselow, M. S. (2005) Dorsal hippocampus NMDA receptors differentially mediate trace and contextual fear conditioning. *Hippocampus* **15**, 665–674
45. Mielcarek, M., Seredenina, T., Stokes, M. P., Osborne, G. F., Landles, C., Inuabasi, L., Franklin, S. A., Silva, J. C., Luthi-Carter, R., Beaumont, V., and Bates, G. P. (2013) HDAC4 does not act as a protein deacetylase in the postnatal murine brain *in vivo*. *PLoS One* **8**, e80849
46. Yu, Y., Wang, H., Rao, X., Liu, L., Zheng, P., Li, W., Zhou, W., Chai, T., Ji, P., Song, J., Wei, H., and Xie, P. (2021) Proteomic profiling of lysine acetylation indicates mitochondrial dysfunction in the hippocampus of gut microbiota-absent mice. *Front. Mol. Neurosci.* **14**, 594332
47. Neumann, H., Peak-Chew, S. Y., and Chin, J. W. (2008) Genetically encoding N(epsilon)-acetyllysine in recombinant proteins. *Nat. Chem. Biol.* **4**, 232–234

48. Li, M., Luo, J., Brooks, C. L., and Gu, W. (2002) Acetylation of p53 inhibits its ubiquitination by Mdm2. *J. Biol. Chem.* **277**, 50607–50611
49. Patton, B. L., Molloy, S. S., and Kennedy, M. B. (1993) Autophosphorylation of type II CaM kinase in hippocampal neurons: Localization of phospho- and dephosphokinase with complementary phosphorylation site-specific antibodies. *Mol. Biol. Cell* **4**, 159–172
50. Saito, K., Hatsugai, N., Horikawa, K., Kobayashi, K., Matsu-Ura, T., Mikoshiba, K., and Nagai, T. (2010) Auto-luminescent genetically-encoded ratiometric indicator for real-time Ca2+ imaging at the single cell level. *PLoS One* **5**, e9935
51. Salomon-Ferrer, R., Gotz, A. W., Poole, D., Le Grand, S., and Walker, R. C. (2013) Routine microsecond molecular dynamics simulations with AMBER on GPUs. 2. Explicit solvent particle mesh ewald. *J. Chem. Theory Comput.* **9**, 3878–3888
52. Min, S. W., Cho, S. H., Zhou, Y., Schroeder, S., Haroutunian, V., Seeley, W. W., Huang, E. J., Shen, Y., Masliah, E., Mukherjee, C., Meyers, D., Cole, P. A., Ott, M., and Gan, L. (2010) Acetylation of tau inhibits its degradation and contributes to tauopathy. *Neuron* **67**, 953–966
53. Pang, Z. P., Cao, P., Xu, W., and Sudhof, T. C. (2010) Calmodulin controls synaptic strength via presynaptic activation of calmodulin kinase II. *J. Neurosci.* **30**, 4132–4142
54. Saunders, A., Macosko, E. Z., Wysoker, A., Goldman, M., Krienen, F. M., de Rivera, H., Bien, E., Baum, M., Bortolin, L., Wang, S., Goeva, A., Nemesh, J., Kamitaki, N., Brumbaugh, S., Kulp, D., *et al.* (2018) Molecular diversity and specializations among the cells of the adult mouse brain. *Cell* **174**, 1015–1030.e1016
55. Mammen, A. L., Kameyama, K., Roche, K. W., and Huganir, R. L. (1997) Phosphorylation of the alpha-amino-3-hydroxy-5-methylisoxazole4-propionic acid receptor GluR1 subunit by calcium/calmodulin-dependent kinase II. *J. Biol. Chem.* **272**, 32528–32533
56. Barria, A., Muller, D., Derkach, V., Griffith, L. C., and Soderling, T. R. (1997) Regulatory phosphorylation of AMPA-type glutamate receptors by CaM-KII during long-term potentiation. *Science* **276**, 2042–2045
57. Takemoto, K., Iwanari, H., Tada, H., Suyama, K., Sano, A., Nagai, T., Hamakubo, T., and Takahashi, T. (2017) Optical inactivation of synaptic AMPA receptors erases fear memory. *Nat. Biotechnol.* **35**, 38–47
58. Penn, A. C., Zhang, C. L., Georges, F., Royer, L., Breillat, C., Hosy, E., Petersen, J. D., Humeau, Y., and Choquet, D. (2017) Hippocampal LTP and contextual learning require surface diffusion of AMPA receptors. *Nature* **549**, 384–388
59. Lee, S. J., Escobedo-Lozoya, Y., Szatmari, E. M., and Yasuda, R. (2009) Activation of CaMKII in single dendritic spines during long-term potentiation. *Nature* **458**, 299–304
60. Hansen, B. K., Gupta, R., Baldus, L., Lyon, D., Narita, T., Lammers, M., Choudhary, C., and Weinert, B. T. (2019) Analysis of human acetylation stoichiometry defines mechanistic constraints on protein regulation. *Nat. Commun.* **10**, 1055
61. Zhang, H. L., Han, W., Du, Y. Q., Zhao, B., Yang, P., and Yin, D. M. (2021) SRC3 acetylates calmodulin in the mouse brain to regulate synaptic plasticity and fear learning. *J. Biol. Chem.* https://doi.org/10.1016/j.jbc.2021.101044
62. Shonesy, B. C., Jalan-Sakrikar, N., Cavener, V. S., and Colbran, R. J. (2014) CaMKII: A molecular substrate for synaptic plasticity and memory. *Prog. Mol. Biol. Transl. Sci.* **122**, 61–87
63. Strack, S., McNeill, R. B., and Colbran, R. J. (2000) Mechanism and regulation of calcium/calmodulin-dependent protein kinase II targeting to the NR2B subunit of the N-methyl-D-aspartate receptor. *J. Biol. Chem.* **275**, 23798–23806
64. Marks, C. R., Shonesy, B. C., Wang, X., Stephenson, J. R., Niswender, C. M., and Colbran, R. J. (2018) Activated CaMKIIalpha binds to the mGlu5 metabotropic glutamate receptor and modulates calcium mobilization. *Mol. Pharmacol.* **94**, 1352–1362
65. Perfitt, T. L., Wang, X., Dickerson, M. T., Stephenson, J. R., Nakagawa, T., Jacobson, D. A., and Colbran, R. J. (2020) Neuronal L-type calcium channel signaling to the nucleus requires a novel CaMKIIalpha-Shank3 interaction. *J. Neurosci.* **40**, 2000–2014
66. Bliss, T. V., and Collingridge, G. L. (1993) A synaptic model of memory: Long-term potentiation in the hippocampus. *Nature* **361**, 31–39
67. Maren, S., Phan, K. L., and Liberzon, I. (2013) The contextual brain: Implications for fear conditioning, extinction and psychopathology. *Nat. Rev. Neurosci.* **14**, 417–428
68. Tovote, P., Fadok, J. P., and Luthi, A. (2015) Neuronal circuits for fear and anxiety. *Nat. Rev. Neurosci.* **16**, 317–331
69. Kim, W. B., and Cho, J. H. (2017) Encoding of discriminative fear memory by input-specific LTP in the amygdala. *Neuron* **95**, 1129–1146.e1125
70. Rogan, M. T., Staubli, U. V., and LeDoux, J. E. (1997) Fear conditioning induces associative long-term potentiation in the amygdala. *Nature* **390**, 604–607
71. Grunwald, M. E., Zhong, H., Lai, J., and Yau, K. W. (1999) Molecular determinants of the modulation of cyclic nucleotide-activated channels by calmodulin. *Proc. Natl. Acad. Sci. U. S. A.* **96**, 13444–13449
72. Yao, X., Zhang, M., Wang, X., Ying, W., Hu, X., Dai, P., Meng, F., Shi, L., Sun, Y., Yao, N., Zhong, W., Li, Y., Wu, K., Li, W., Chen, Z. J., *et al.* (2018) Tild-CRISPR allows for efficient and precise gene knockin in mouse and human cells. *Dev. Cell* **45**, 526–536.e525
73. Kameyama, K., Lee, H. K., Bear, M. F., and Huganir, R. L. (1998) Involvement of a postsynaptic protein kinase A substrate in the expression of homosynaptic long-term depression. *Neuron* **21**, 1163–1175
74. Biber, A., Schmid, G., and Hempel, K. (1984) Calmodulin content in specific brain areas. *Exp Brain Res.* **56**, 323–326
75. West, P. J., Saunders, G. W., Remigio, G. J., Wilcox, K. S., and White, H. S. (2014) Antiseizure drugs differentially modulate theta-burst induced long-term potentiation in C57BL/6 mice. *Epilepsia* **55**, 214–223
76. Kouvaros, S., and Papatheodoropoulos, C. (2016) Theta burst stimulation-induced LTP: Differences and similarities between the dorsal and ventral CA1 hippocampal synapses. *Hippocampus* **26**, 1542–1559